

FLOWAGE DIFFERENTIATION IN

ULTRAMAFIC SILLS OF UNGAVA, P.Q.

FLOWAGE DIFFERENTIATION  
IN THE  
ULTRAMAFIC SILLS  
OF THE  
CAPE SMITH-WAKEHAM BAY FOLD BELT, UNGAVA, P.Q.

By  
DANNY LEE THOMPSON

Submitted to the Department of Geology  
in Partial Fulfilment of the Requirements  
for the Degree  
Honours Bachelor of Science

McMaster University

April, 1976

HONOURS BACHELOR OF SCIENCE (1976)  
(Geology)

McMASTER UNIVERSITY  
Hamilton, Ontario.

TITLE: Flowage Differentiation in the Ultramafic Sills  
of the Cape Smith - Wakeham Bay Fold Belt, Ungava, P.Q.

AUTHOR: Danny Lee Thompson

SUPERVISOR: Professor P. M. Clifford

NUMBER OF PAGES: xi, 100

#### ABSTRACT

An intrusive Ultramafic sill of the Cape Smith-Wakeham Bay Fold Belt, located in the Ungava Peninsula P.Q., was studied. Measurements of olivine crystals were made on enlarged images of thin sections to determine the average olivine grain size and volume across the intrusion.

The Bravo ultramafic sills exhibit a peculiar petrographic and chemical zoning, the rocks becoming increasingly rich in olivine as one moves toward the centre of the intrusion. Rock Compositions range from gabbro at the margin to olivine rich peridotite near the centre. The olivine grain size distribution exhibits a similar zoning, the grain size increasing toward the centre. However, the maximum value is skewed

somewhat to the south along the edge of the central olivine rich zone, coinciding with the maximum value of  $N_s$  (Nickel in sulfides).

The zoning is a consequence of flowage differentiation. Along the margins of the intrusion grain dispersive pressure (the pressure due to mechanical interaction between phenocrysts) is dominant and grains are forced toward the centre. Within the centre of the intrusion, where the increased crystal concentration results in plug flow, the force of gravity is dominant and the largest grains make their way to the base of the plug.

The Bravo Ultramafic Sills are pre-tectonic in origin being intruded into a group of eugeosynclinal strata in a sub-horizontal attitude.

Plate 1 Ungava, June 1, 1975

Plate 2 Home Sweet Home!



### ACKNOWLEDGEMENTS

First, and foremost, the writer would like to express his gratitude to Cominco Ltd. for allowing collection of field data and samples during the 1975 field season and for providing chemical analyses and thin sections of the rocks studied. Also, thanks goes to Cominco geologists: D. Ransom, A. Ouellet and I. Mason, for helpful discussion while in the field.

Guidance and helpful advice were provided by the Author's thesis supervisor, P. M. Clifford. I am especially grateful for his critical reading of the manuscript. Thanks goes to J. Whorwood for photographic reduction of charts and maps and general drafting advice. Mrs. Greer typed the manuscript with speed and precision. I am extremely grateful for her assistance.

Last, but certainly not least, I would like to thank my wife for making most of the 7,000 olivine grain measurements essential to my analysis; and for her unending encouragement throughout the preparation of this thesis.

## CONTENTS

	page no.
ABSTRACT	ii
ACKNOWLEDGEMENTS	vi
CHAPTER I	
A. INTRODUCTION	1
B. STATEMENT OF PROBLEM AND METHOD OF STUDY	3
CHAPTER II	
A. GEOLOGICAL SETTING	6
B. FIELD RELATIONS OF BRAVO ULTRAMAFIC SILLS	8
C. FIELD AND PETROGRAPHIC DESCRIPTION OF BRAVO ULTRAMAFICS	17
i) INTRODUCTION	
ii) CONTACT ZONE	
iii) BORDER ZONE	
iv) INTERMEDIATE ZONE	
v) CENTRAL ZONE	
vi) OLIVINE ABUNDANCE	
D. CHEMICAL ANALYSES	27
CHAPTER III	
GRAIN SIZE ANALYSIS	32
i) INTRODUCTION	
ii) DISCUSSION AND RESULTS	

CHAPTER IV	
FLOWAGE DIFFERENTIATION	47
CHAPTER V	
A. DISCUSSION	59
B. SUMMARY AND CONCLUSIONS	68
REFERENCES	70
APPENDICES	75

## FIGURES

	page no.
1. Location Map - Cape Smith - Wakeham Bay Belt.	5
2. Geology of Bravo Ultramafics.	9
3. % Modal Olivine	26
4. Chemical Analyses of Bravo Ultramafics.	29
5. Variation in Olivine Grain Size (after Gibb 1968).	33
6. Length, Area, Volume Relations.	35
7. Grain Size Distribution Class Interval $.13\text{mm}^2$ .	37
8. Grain Size Distribution Class Interval $.065\text{mm}^2$ .	38
9. Grain Size Distribution Class Interval $.0325\text{mm}^2$ .	39
10. Average Grain Area and Volume.	40
11. Histogram Modal Values.	41
12. M-factor 10.	42
13. M-factor 30.	43
14. M-factor 50.	44
15. Crystal Concentration for Various Fluids of Increasing Non-Newtonian Character.	54
16. Example of Crystal Concentration, Shear Stress and Velocity Profile, for a Wall Concentration of 10% and Maximum Velocity U.	55
17. Crystal Concentrations for Various Initial Wall Concentrations (assuming modified analysis, see text).	56

18. Gravity Skewed Concentration Profile	58
19. Schematic Representation of Original Olivine Distribution	61
20. Force Distribution During Flow.	63
21. Force Distribution within Bingham Fluid.	66

PLATES

	page no.
1. Ungava, June 1, 1975	v
2. Home Sweet Home!	v
3. Air Photo of Study Area	12
4. Peridotite Outcrop	12
5. Contact of Intrusive with Country Rock	14
6. Country Rock near Sill Termination	14
7. Tight folding in Country rocks near sill termination	16
8. Photomicrograph of pyroxene from border zone	22
9. Photomicrograph of poikilitic pyroxene	22
10. Photomicrograph of Tremolite - Bastite alteration	24
11. Photomicrograph of olivine pseudomorphs	24

## CHAPTER I

### A. INTRODUCTION

One of the ultimate purposes of geologic research is to be able to predict the result of natural processes, or from another point of view, to be able to specify the environment(s) in which a rock evolved. There are two basic approaches to such problems:

1. Make field observations - construct a model. Continue observations suggested by features of the model - refine the model in the light of new data.
2. Consider possible earth processes - add reasonable boundary conditions. What is the result? Look for it!

Advances in geology are based on the first approach; method two is uncommon. Consider for a moment turbidite sedimentation. Anyone who has watched muddy water flow into clear water should have been able to predict the existence of turbidity currents along continental margins. However, the scale of the process is so removed from normal human experience, that it was not until numerous direct observations had been made, that the turbidite model was proposed. Admittedly the second approach is difficult.

The substance of this thesis is along the lines of approach one, step two--additional observation to refine a pre-existing model, or, to be more precise, "a demonstration that flowage differentiation was an important process in the evolution of the ultramafic intrusions of the Cape Smith-Wakeham Bay Belt". The initial comments were added because

flowage differentiation is a process which was not predicted, but which should have been predictable. We know that magmas flow during intrusion; does this effect the final result? Observations of intrusions exhibiting evidence of flowage differentiation have been explained in a variety of ways; for example multiple intrusion has been appealed to. Eventually enough unexplainable observations were made (in terms of known processes) that the possible processes occurring during intrusion of a crystal mush were investigated experimentally. These model experiments indicated that flowage differentiation was a very likely and significant process. Since this initial realization, a number of field studies have confirmed this view.

## B. STATEMENT OF PROBLEM AND METHOD OF STUDY

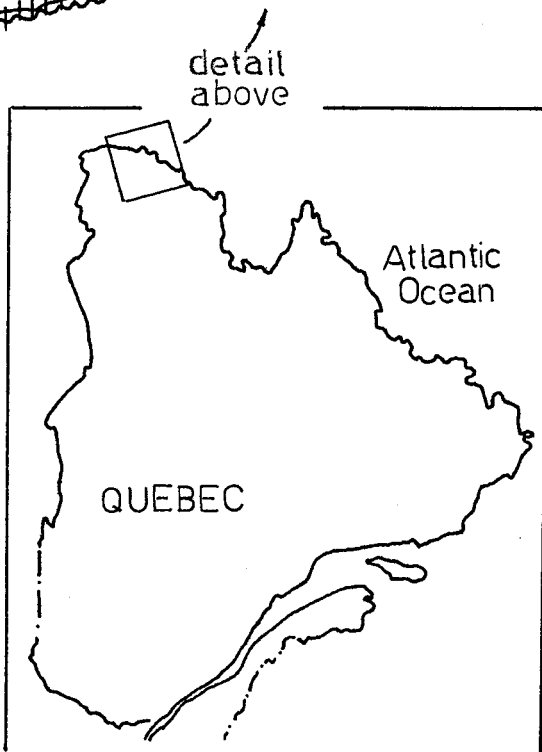
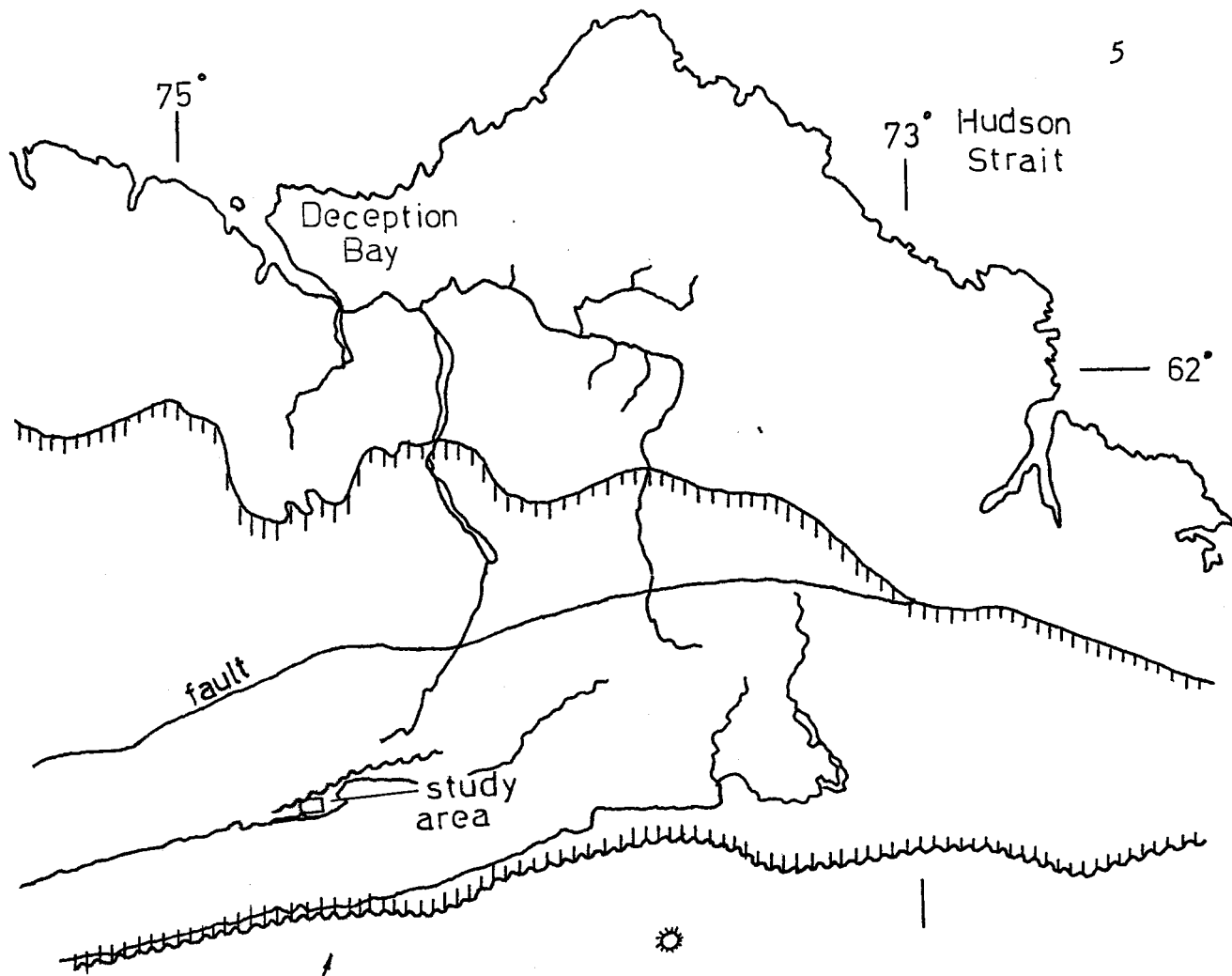
During the 1975 field season the author was employed by COMINCO Ltd. as part of the Kenty Lake project in the Cape Smith - Wakeham Bay Fold Belt. The exploration for Cu-Ni sulfides in differentiated ultramafic intrusives raised a number of questions concerning their evolution, for example, how did the sills (dikes?) develop their peculiar zoning and why do the sulfide bodies commonly occur only along one side? The possibility of flowage differentiation being responsible was a common topic of discussion, however little data existed to prove the case one way or the other.

The purpose of this thesis is to provide grain size data and petrographic data across one intrusive, which may be compared with the existing chemical analyses made by COMINCO. This will allow determination of the significance of flowage differentiation as the process producing the zoning visible in these bodies.

Approximately 100 thin sections were examined, out of which 13 were chosen for grain size analysis across the main ultramafic body on Bravo grid (see fig.2). Measurements of individual olivine crystals were made by hand with a ruler on a projected image of the thin section. The number of measurements ranged from 200 to 450 per thin section, depending on the abundance of olivine and the quality of the thin section. These measurements were then used to approximate the original volume of the grains and to construct histograms of grain size across the intrusive. % modal olivine has been determined from thin sections using standard

point counting methods.

The intrusives studied are here after referred to as the Bravo  
Ultramafic sills.



## CAPE SMITH WAKEHAM BAY BELT

-  OUTLINE OF BELT
-  UNCONFORMITY

Fig.1

## CHAPTER II

### A. GEOLOGICAL SETTING

The Cape Smith-Wakeham Bay Fold Belt forms part of the Circum-Ungava geosyncline which surrounds the Ungava craton in a wide open arc to the south. The geology of the Belt is known largely from a series of reports by the Quebec Department of Natural Resources (Bergeron, 1959; Beal, 1959, 1960; and Gelinis, 1962) which cover chiefly the central part of the Belt and more recently by detailed GSC mapping and stratigraphic studies (Baragar 1974). The Belt lies within the Churchill structural province and is Archean in age (Rb-Sr dates around 1800 my from sediments; Fryer, 1970; in Davidson, 1972).

The eugeosynclinal strata display tight longitudinal folds and are divided roughly into two sections by a major east-west trending fault. The major stratigraphic divisions of the southern section are: 1) a lower sedimentary unit of quartzites, dolomites and shales that rest unconformably on gneisses of the Archean basement; 2) a lower volcanic unit comprising massive volcanic flows with interbedded shales and quartzites invaded by thin doleritic sills; 3) an upper sedimentary unit composed of quartzites, quartzite breccias and conglomerates and/or shales and minor volcanic breccias and pillow lava; and 4) an upper volcanic unit consisting chiefly of pillowed mafic lavas (Baragar, 1974). The entire sequence is intruded by numerous mafic and ultramafic sills. Rocks north of the fault include mafic schists and metasediments which might reasonably be interpreted as the metamorphosed equivalents of the

rocks to the south.

A major period of deformation and metamorphism reached its peak about 1600-1700 my ago (k-Ar mica age; Wanless, 1970 in Davidson, 1972) during the Hudsonian Orogeny. In general metamorphism increases from the lower greenschist facies in the south to the amphibolite facies in the north where the schistose mafic rocks continue northward into gneisses of uncertain derivation.

It has been suggested (Baragar, 1974) that the sequence probably represents facies changes from south to north or from landward to seaward in a geoclinal basin.

### B. FIELD RELATIONS OF BRAVO ULTRAMAFIC SILLS

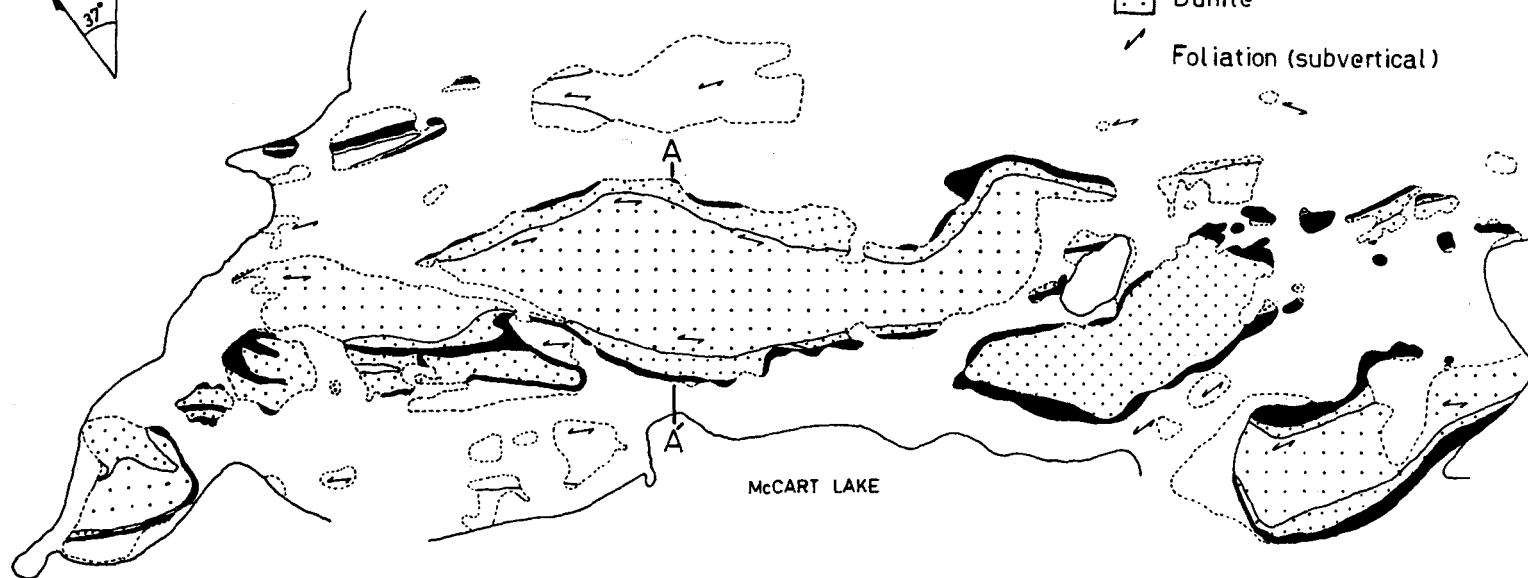
The major field relations of the Bravo Ultramafic sills are illustrated in fig. 2. Although there are numerous individual outcrops, magnetic mapping indicates the presence of only 3 or 4 continuous bodies just below the surface. These bodies are usually lensoid in shape with tapered or blunt terminations. They vary from 100 to 500 meters in thickness, averaging approximately 300 meters, and may be fairly irregular. The largest sill can be traced with certainty, for a little over 3.3 kms., however, as it is on strike with similar bodies it may actually extend for several 10's of kms. The sills are intruded into a variable mixture of sediments which weather as topographic lows and outcrop less abundantly than the intrusive. Although contacts with the country rock are invariably overlain by frost heaved rubble and glacial till, overall structure suggests that the sills are steeply dipping to the north and predominantly concordant with the foliation in the surrounding rock. This foliation can be shown to be at a high angle to bedding in certain locations (Wolf 1974). Therefore the sills may be discordant to the original sedimentary bedding. However, these relations are by no means clear.

The sediments are typically thinly bedded slates and graywackes with lesser carbonate and quartz rich graywacke lenses. Metamorphism is of the low grade type (Winkler 1974). Most outcrops are characterized by fairly tight folding and development of a prominent cleavage and/or lineation. Folds within small carbonate bands are commonly

Fig.2 GEOLOGY OF BRAVO ULTRAMAFICS  
Ungava PQ

LEGEND

-  Sediments
-  Pyroxenite
-  Peridotite
-  Dunite
-  Foliation (subvertical)



McCART LAKE

Scale in meters



Geology by A.S. Ouellet 1974  
and D.L. Thompson 1975

strongly flattened and the noses boudinaged. At one location near a sill termination, the slate is characterized by development of several intersecting cleavages which break the rock into small parallelograms.

The role played by the sills in the development of the structural features within the sediments is unknown. Analyses by Johnson et al (1973), Pollard et al (1973), and Pollard (1973) indicate that many of these features, in particular the large number of intersecting cleavages, is a common and predictable feature associated with the emplacement of sills. If we may anticipate the conclusions of this study which suggest the sills are pre-deformation, then it is likely that they controlled the formation of some of these structures simply by their presence.

Plate 3 Looking west along strike of ultramafic bodies. Location of grain analysis is indicated by A-A'.

Plate 4 Typical outcrop of rough, rusty weathering peridotite. Note the magnetite foliation as indicated by the dark bands. Hammer for scale.



Plate 5 Contact of intrusive with country rock  
(dotted line). Hammer for scale.

Plate 6 Country rock near sill termination. It is  
characterized by a number of intersecting cleavages  
not found at other locations. Scale is 15 cm. long.



Plate 7 Tight folding in country rocks near sill  
termination. Hammer for scale.



## C. FIELD AND PETROGRAPHIC DESCRIPTION OF BRAVA ULTRAMAFICS

### i) INTRODUCTION

The Bravo sills are differentiated ultramafic sills. They exhibit a strong megascopic zoning parallel to their contacts (Wolf 1974), similar to that noted by Fahrig (1962). The zoning is roughly symmetrical about the central axis of the intrusive, dividing it into four distinct lithologic units:

1. Contact Zone (rodingite)
2. Border Zone (meta-pyroxenite)
3. Intermediate Zone (meta-peridotite)
4. Central Zone (olivine rich meta-peridotite)

The mineralogy of these sills has been very briefly described by Wolf (1974). More detailed descriptions of similar intrusions from the Circum-Ungava fold belt have been made by Beall (1959), Fahrig (1962) and Robertson (1975). The descriptions given here are based on the author's own observations. However, suggested mineral compositions and interpretations lean heavily on the ideas of the above authors.

### ii) CONTACT ZONE

Easily observable contacts with the country rocks are uncommon, as was mentioned above. When found they are characterized by a thin selvage of rodingite. This is a metasomatic alteration product of the country rock, rich in calcium-aluminum silicates, and is therefore not actually part of the intrusive. In the best example examined by the author, the sill has intruded an original banded siltstone. Away

from the contact this rock is composed of fine grained clastic quartz and muscovite, indicative of lower greenschist facies metamorphism. Close to the contact the siltstone is a light whitish brown, sugary textured, massive band, approximately 30 cm. wide with gradational borders. The mineralogy is characterized by development of prehnite, clinozoisite, white mica and quartz-diopside porphyroblasts.

At another location the contact is characterized by a greenish coloured biotite hornfels, composed of fine grained quartz, chlorite, white mica, magnetite and large poikilitic biotites. Due to the nature of the outcrop, the location of this sample with respect to the sill contact is not clear, nor is the identification of the country rock from which it was derived. It is interesting to note that the biotite shows no indication of deformation. This would suggest the hornfels may have formed after the regional deformation.

### iii) BORDER ZONE

The border zone is the outermost zone of the actual intrusion. It occurs as a rather massive band varying from 10 to 100 meters in width and weathering to a mottled light, sometimes whitish, green. The surface is commonly shiny and appears sheared in places. This is probably the result of glacial action or weathering. The original rock was a pyroxenite, consisting almost entirely of interlocking pyroxene crystals, now altered to a tremolite-actinolite assemblage with lesser amounts of talc and serpentine minerals. Olivine, now altered to tremolite, is locally present up to 10%, having been

poikilitically enclosed by original pyroxene.

At several locations, the extreme border phase in contact with the country rock is gabbroic in nature. Such occurrences are very narrow and in general, plagioclase was a minor constituent in the original intrusion.

#### iv) INTERMEDIATE ZONE

With an increase in the olivine content the border zone grades into the intermediate zone or peridotite zone. This transition is everywhere gradational and there is no textural evidence of gravitative settling. The peridotite weathers to a reddish brown colour with large pyroxene phenocrysts standing out on the surface giving it a rough, knobby appearance. During field mapping this zone was arbitrarily identified by the occurrence of such rusty coloured peridotite; it corresponds roughly to the presence of modal olivine in the range 20-60%.

The fresh surface of this rock is typically dark bluish green with the pyroxenes appearing as whitish green patches. Original olivine is not present in these rocks; it has been completely altered to serpentine (antigorite) plus lesser amphibole and chlorite. However, pseudomorphous relict textures indicate that the original olivine occurred as distinct euhedral to rounded crystals poikilitically enclosed by pyroxene. Pyroxene is probably the only other major mineral that was present in the original intrusion. Although it is still present as endiopside (pyroxene being more resistant to serpentinization than olivine), a significant proportion has been altered to amphibole or

chlorite minerals. The amphibole minerals include large patches of optically continuous tremolite-actinolite and lesser amounts of pleochroic brown hornblende. Fahrig (1962) considers the hornblende an intermediate step in the alteration process between the pyroxenes and the tremolite-chlorite assemblage. A less common but significant alteration product is patches of tiny, fibrous, unoriented tremolite surrounded by interstitial serpentine (bastite). The chlorite minerals include serpentine (antigorite) and penninite, the latter being restricted to the groundmass in most cases.

An important accessory, commonly in the order of 10%, is sub-hedral magnetite. Although it is particularly associated with serpentine, it occurs almost everywhere and is sometimes concentrated into thick linear patches. On outcrop scale, fine bands of magnetite (0.1 to 1 cm. in width) define a well developed foliation which is predominantly subparallel to the sill contact.

#### v) CENTRAL ZONE

The central zone, although mapped as dunite, originally contained a maximum of 75% olivine and would be better termed an olivine-rich peridotite. This rock is now properly termed a serpentinite, all primary olivine being completely altered to serpentine. In outcrop it appears massive and weathers to a tan or dark greenish colour. The fresh surface is black or very dark green and large pyroxenes are less common than in the intermediate zone. A strong magnetite foliation is commonly present parallel to the gross orientation of the entire intru-

Plate 8 Shows pyroxene from border zone now completely altered to amphibole and talc. Pseudomorphs of olivine (ol) are visible within the larger crystals. Polarized light X 60.

Plate 9 Original pyroxene (py) poikilitically enclosing serpentine after olivine (ol). Note the euhedral (shape) of the olivine. Tremolite (tr) and brown hornblende (hr) are also present. Polarized light X60 .

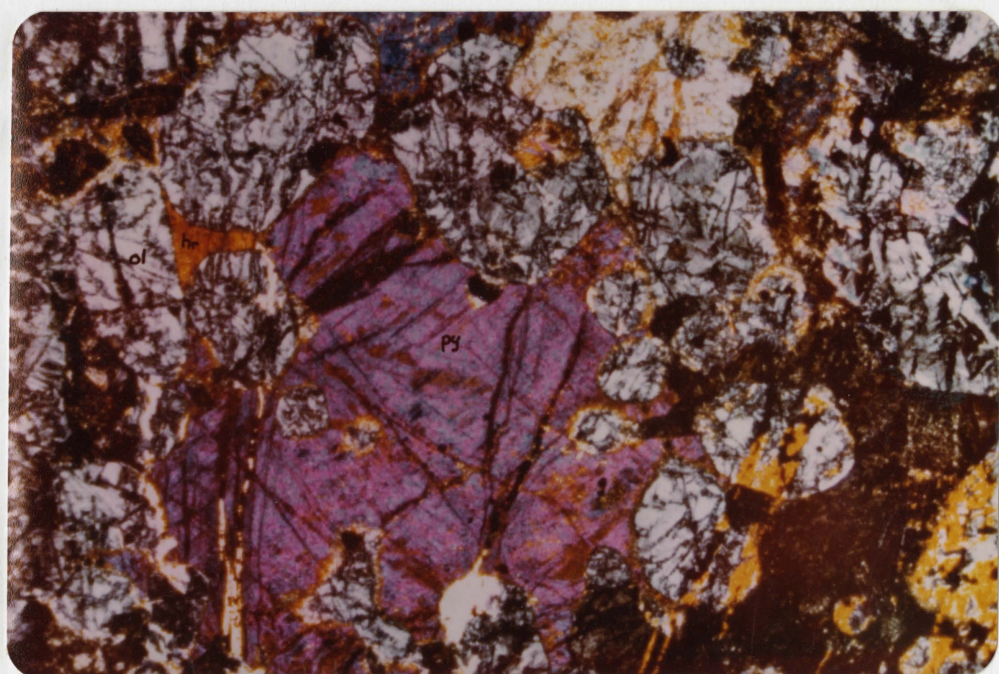
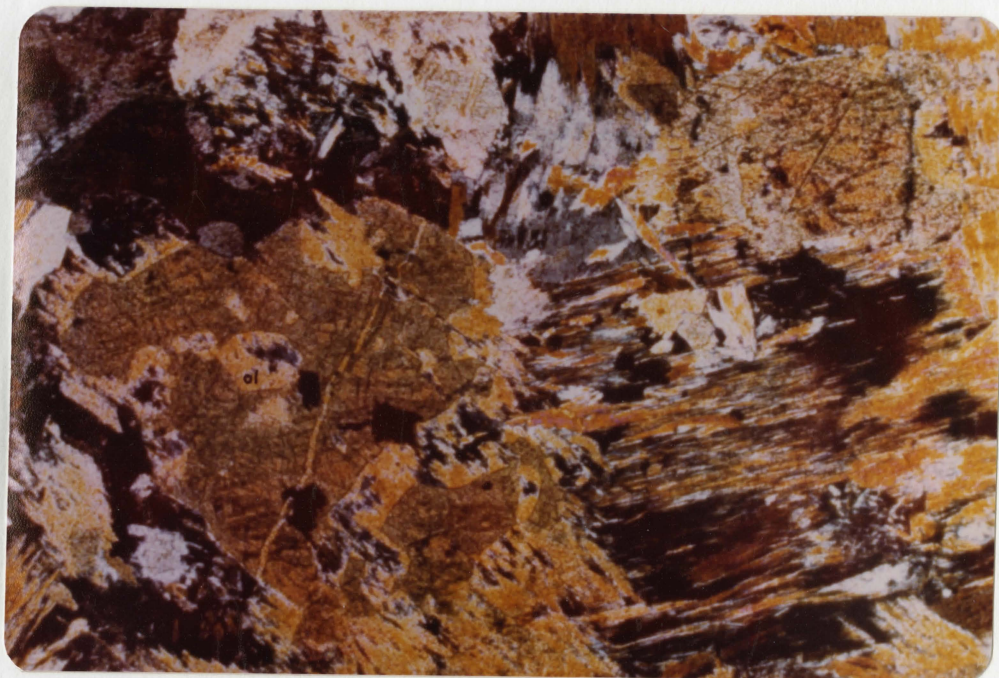
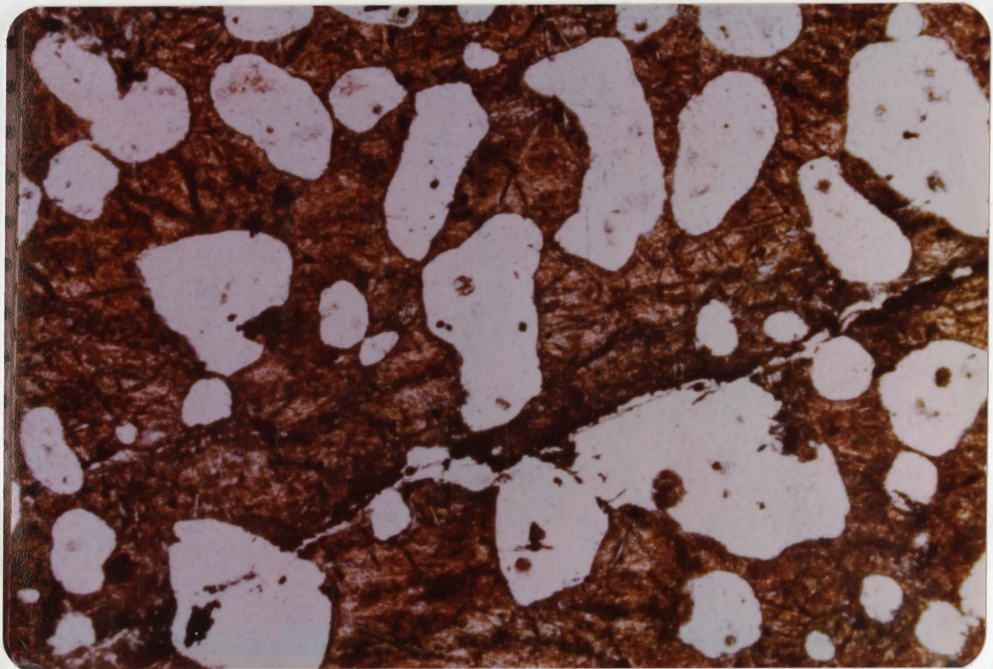
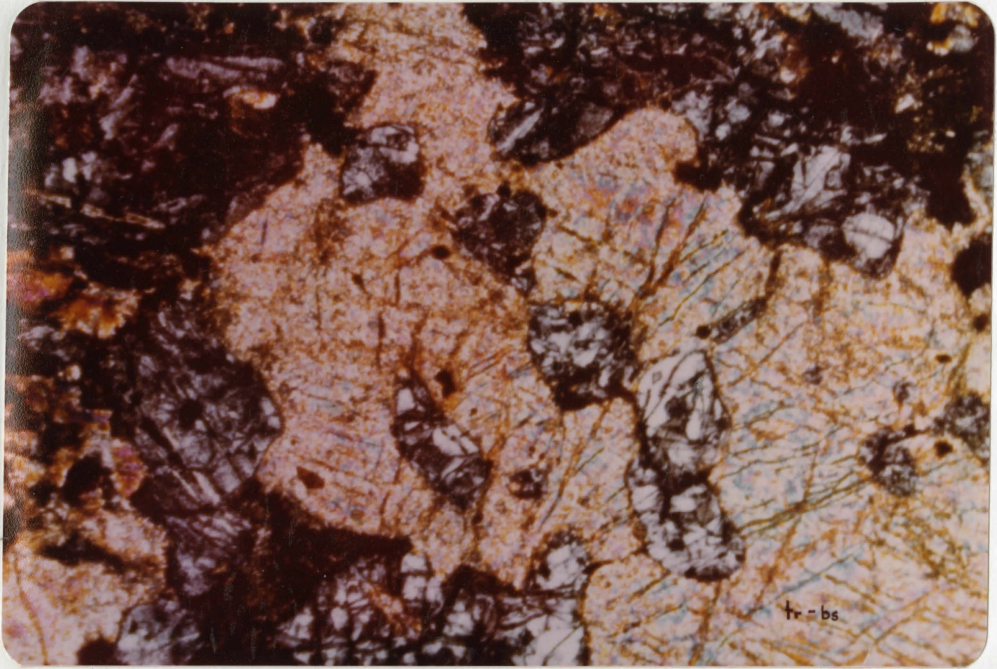


Plate 10 Tremolite-bastite (tr-bs) alteration of  
pyroxene. Polarized light X 60.

Plate 11 Olivine pseudomorphs within altered pyroxene.  
Note the rounded shape and embayments of some of the  
olivine. Plain light X 60.



sive. Magnetite also coats joint surfaces and in several locations forms sets of irregularly oriented intersecting planes which break the outcrop up into small fist sized blocks upon weathering. Small veinlets of brittle crysotile are also common.

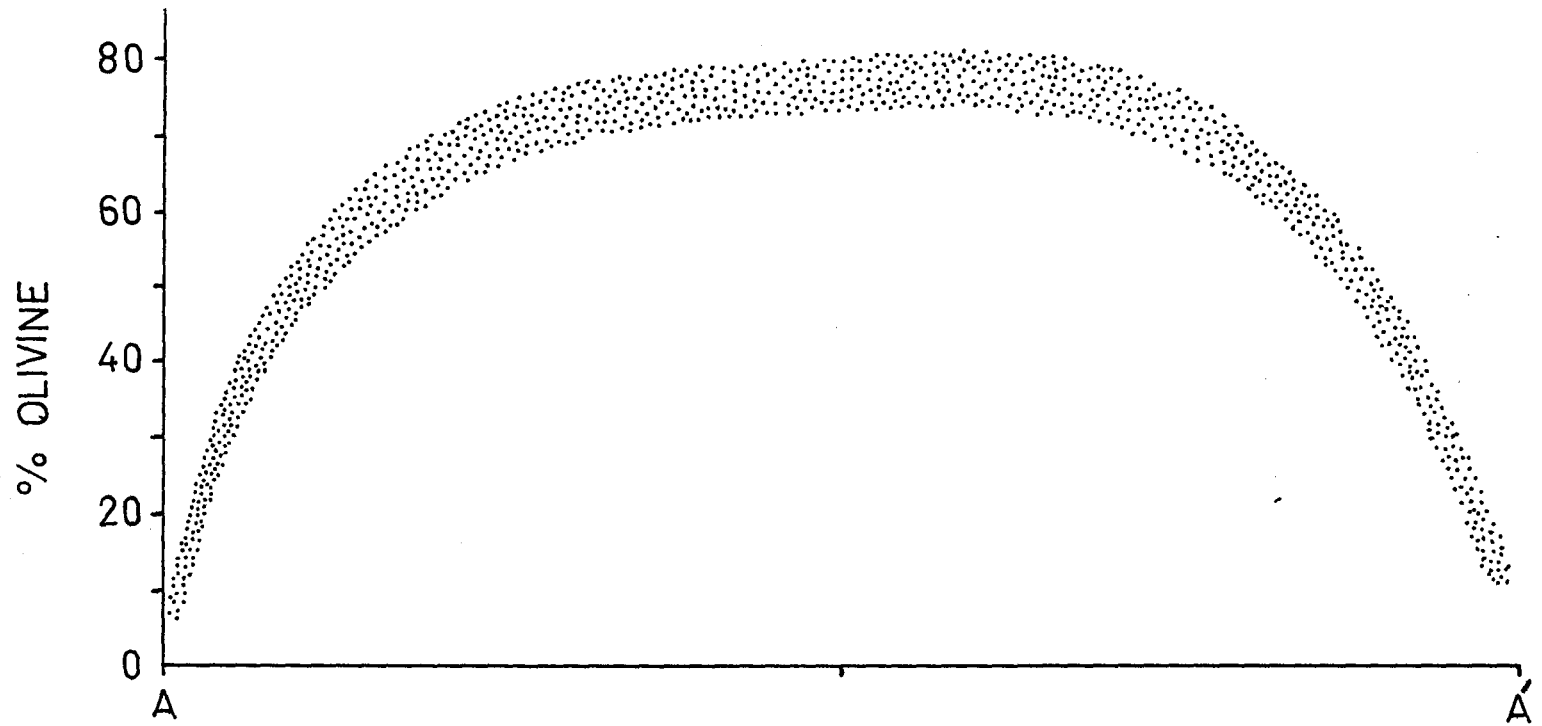
The mineralogy is very similar to that of the intermediate zone but with increased abundance of original olivine. Individual pseudomorphs of serpentine after olivine are now commonly surrounded by a groundmass of fine serpentine and many have lost their original identity. This makes determination of the original mineralogy more difficult than for the intermediate zone.

#### vi) OLIVINE ABUNDANCE

Using pseudomorphous textures to approximate the original mineralogy, the pre-alteration abundance of olivine across the intrusion has been determined by point counting. The results are shown in fig. 3. According to Frangipane (1974), reliability improves with the number of points counted, reaching a limiting value of  $\pm 2.2\%$  at 500, after which increasing the count produces only a small improvement. Additional error arises from the difficulty in distinguishing matrix serpentine from serpentine pseudomorphs of original olivine. The value of this error is unknown but  $\pm 3.3\%$  would seem to be a convenient overestimate as this makes the total error  $\pm 5\%$ .

% MODAL OLIVINE  
cross section A-A'

Fig.3



#### D. CHEMICAL ANALYSES

Chemical analyses of the rocks discussed have been provided by Cominco and are contained in the "Ungava Exploration Year End Report" (Wolf 1974). These analyses have been included due to the significant supporting evidence they contain concerning the mechanism of differentiation. The location and value of the oxides and trace elements analysed are shown in fig. 4. The samples are from the cross-section A-A' shown in fig. 2. Note that only six analyses are given for CaO, Na<sub>2</sub>O, K<sub>2</sub>O, TiO<sub>2</sub> and Al<sub>2</sub>O<sub>3</sub> while 17 analyses are given for MgO, SiO<sub>2</sub>, Fe<sub>t</sub> (Fe total), S, Cu<sub>t</sub>, and Ni<sub>s</sub> (Ni in sulfides). The trends which I consider significant are as follows:

1. CaO, Na<sub>2</sub>O, K<sub>2</sub>O, Cu<sub>t</sub> and TiO<sub>2</sub> show an increase toward the north side of the intrusion.
2. MgO shows a rapid and symmetrical increase toward the central zone, presumably due to the increase in olivine content. The low central value remains unexplained unless due to sampling or analytical errors.
3. Ni<sub>s</sub> shows a rapid increase toward the southern margin of the central zone where it reaches a maximum. It then decreases toward the very outer margin of the intrusion.
4. S content is variable, but it does show a significant peak near the south margin of the central zone which corresponds to the Ni<sub>s</sub> peak. The S increase toward the north may be related to the Cu<sub>t</sub> increase.

In general it is important to note that, overall the intrusion is chemically asymmetric while the continuity of most trends across the intrusion suggests a lack of sharp chemical discontinuities.

CHEMICAL ANALYSES OF BRAVO  
ULTRAMAFICS SECTION A-A'

Fig. 4

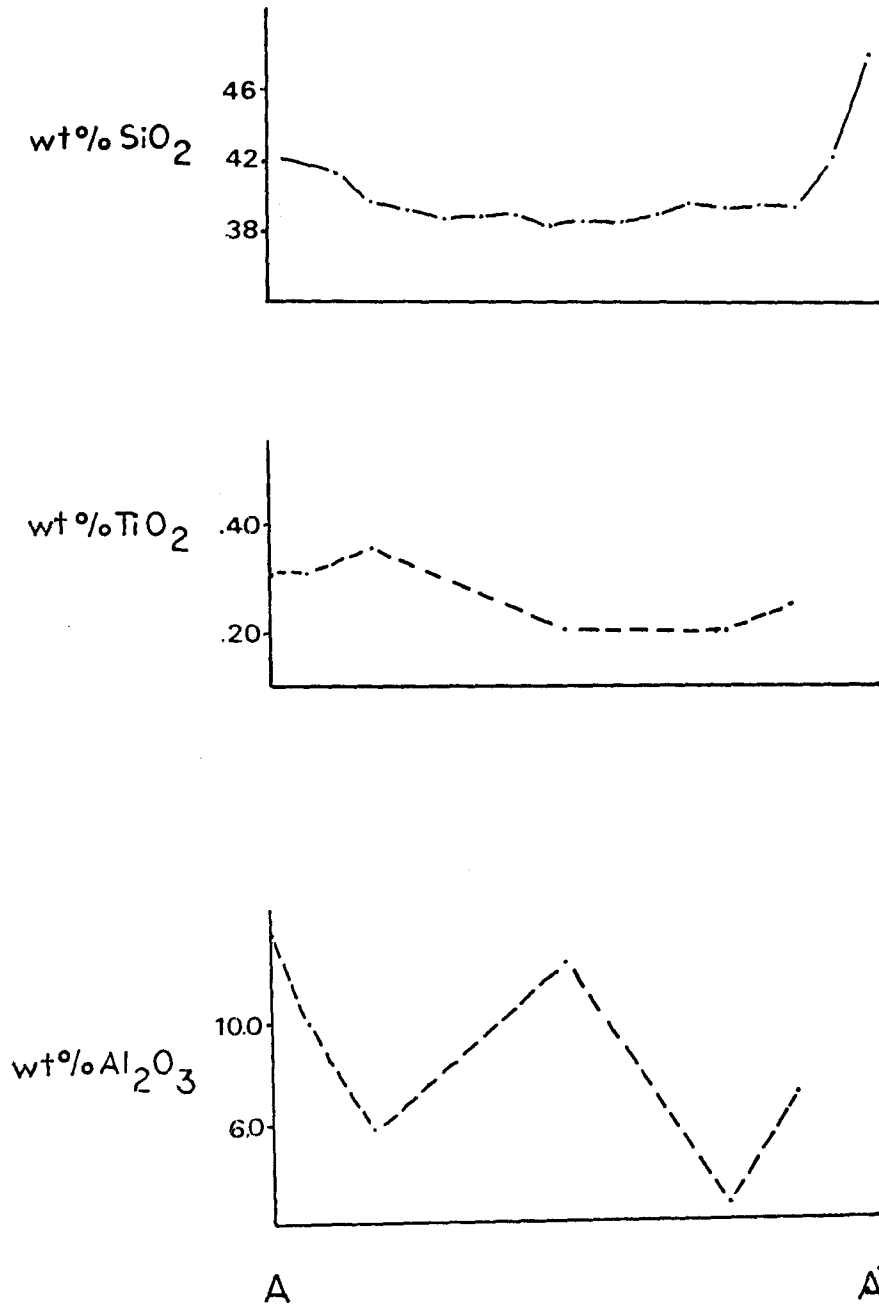


Fig.4 Con't.

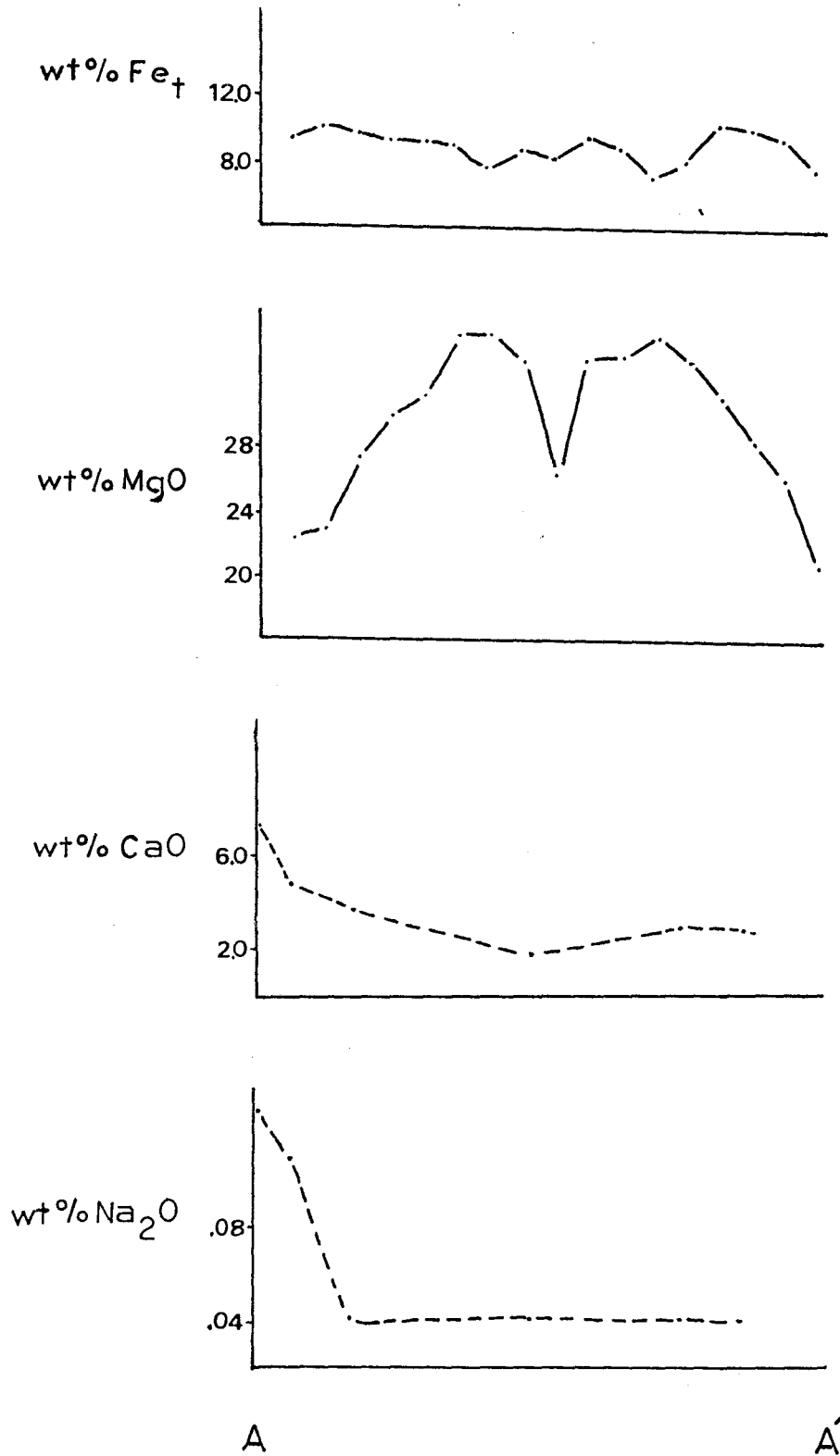
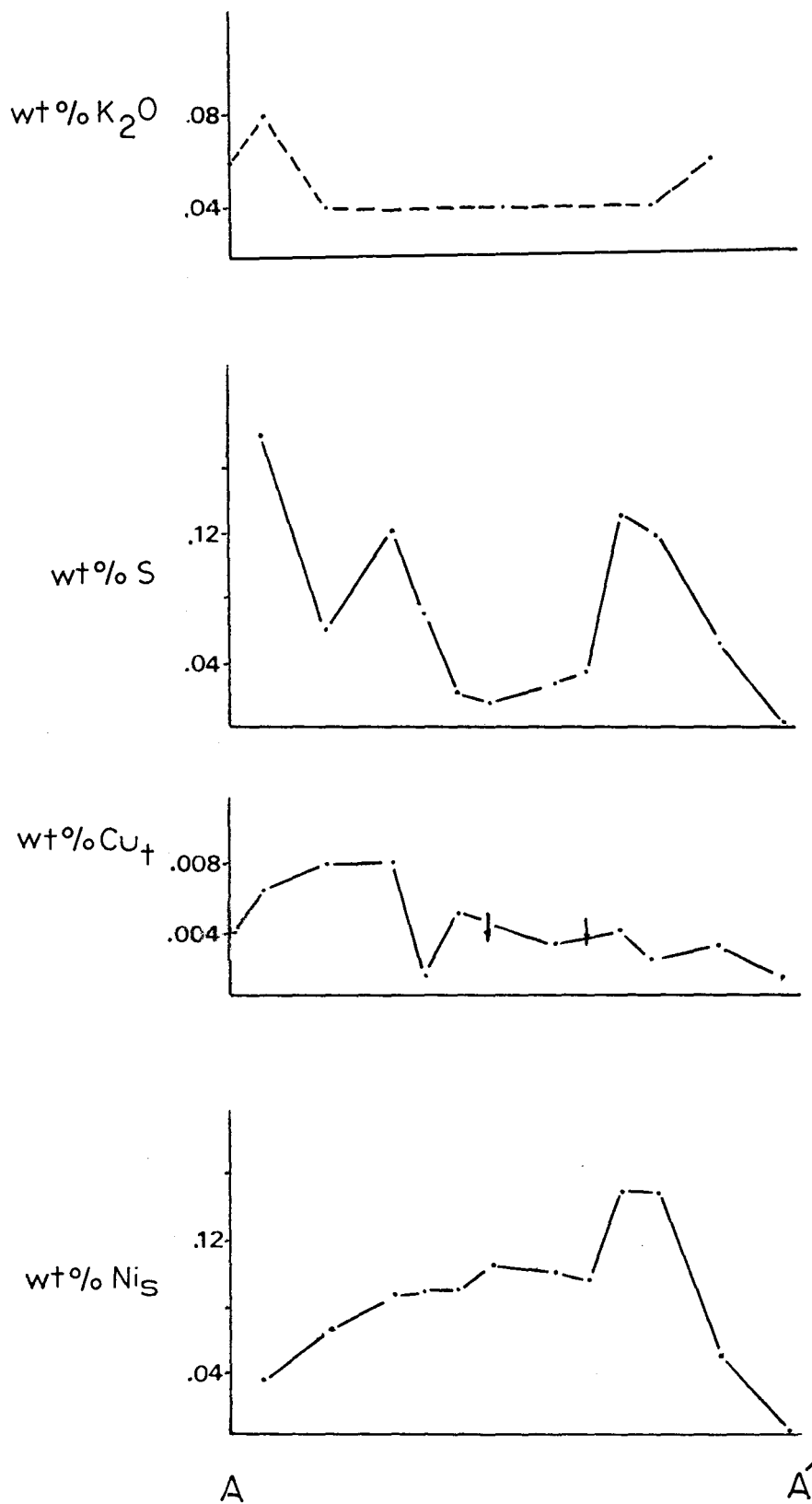


Fig.4 Con't.



## CHAPTER III

### GRAIN SIZE ANALYSIS

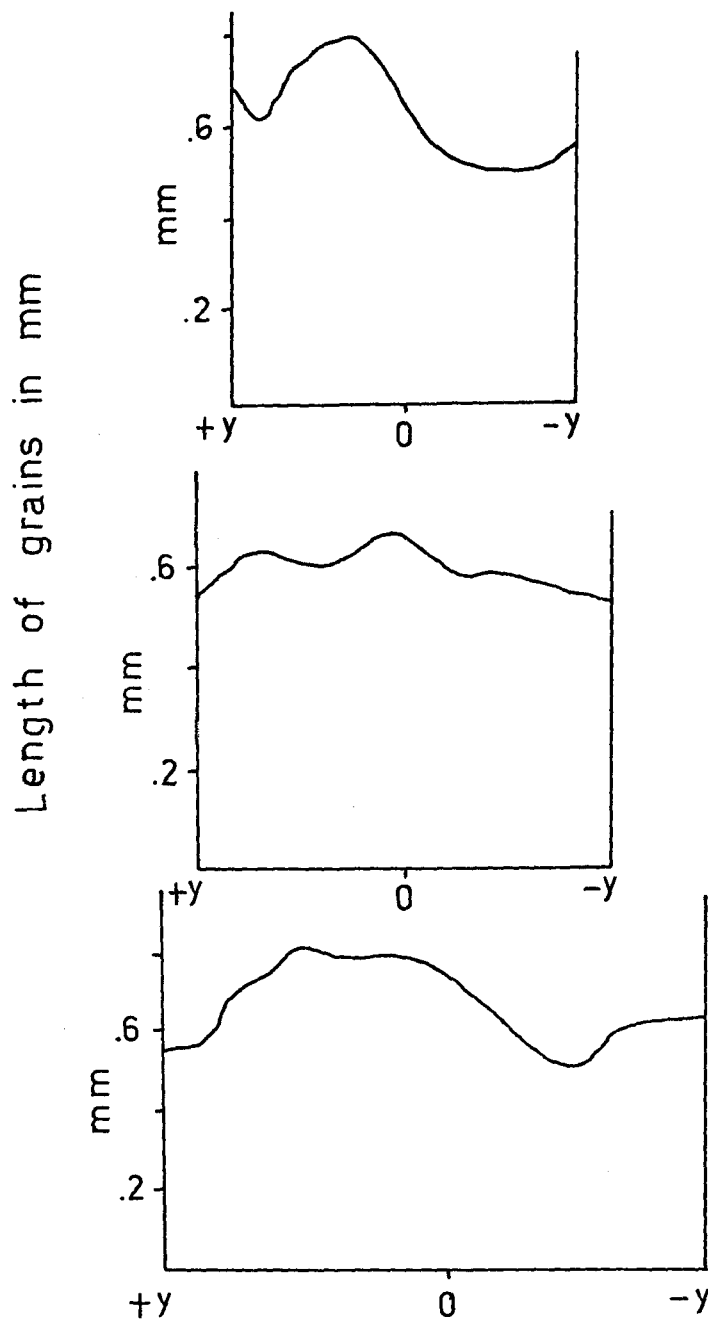
#### i) INTRODUCTION

Systematic variation in olivine grain size is a common feature of intrusive ultramafic bodies (Drever and Johnston, 1967). However, little attempt has been made to quantify the variation.

Semi-quantitative measurements have been made for dikes in Scotland (Gibb, 1968). This study involved measuring the lengths of approximately 1,000 crystals to test, among other things, the notion that bimodal distributions would indicate two distinct generations of olivine. Gibb presents plots of the average size of olivine crystals as a function of  $y$  (the half width of the dike) for several dikes (Fig.5), in which the grain size (length) variation is approximately  $\pm 20\%$  from the average; in other words, a 40% increase in grain size is possible in moving from near the edge toward the centre. The exact method of analysis is not described by Gibb, but he states "(size) - has been investigated by measuring the lengths of over 1,000 crystals" (pg.423). I interpret this to mean that one measurement was made for each grain, this being of the maximum length. The average grain size across the intrusion was apparently calculated by taking the average of the measured lengths at each station.

The procedure used by Gibb may be criticized on the basis that the two forces which may act on the particle, grain dispersive pressure (to be discussed below) and gravity, are dependent of the volume of the

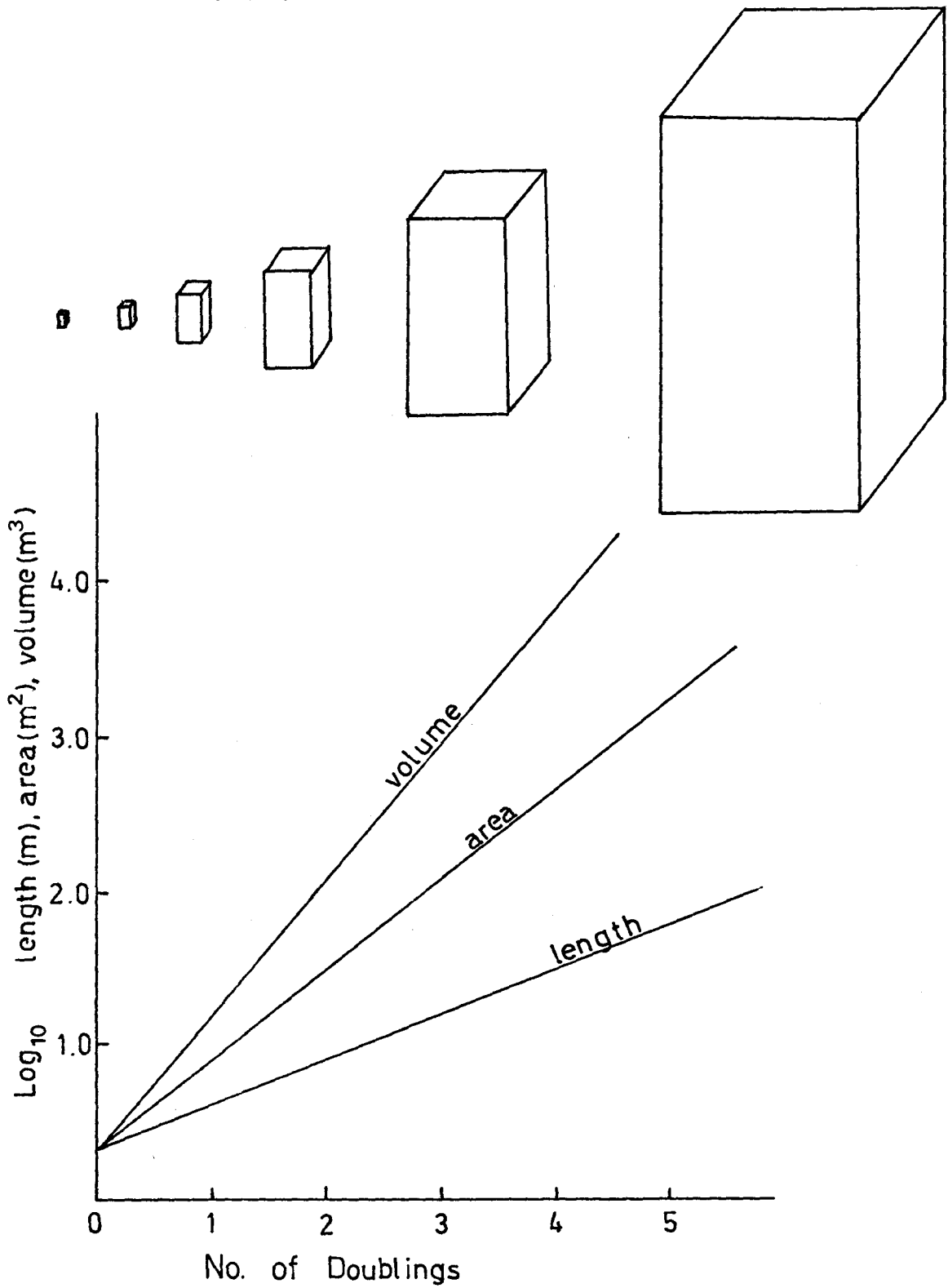
Fig.5 Variation in Olivine Grain Size  
(measurement is of maximum grain  
length - after Gibb 1968 )



particle and not the length. The importance of this consideration is demonstrated in Fig.6. For a grain 1 mm x 1 mm x 2 mm, the length is 2 mm, the area 2 mm<sup>2</sup> and the volume 2 mm<sup>3</sup>. Now consider the same grain if we double the lengths; the length is now 4 mm, the area 8 mm<sup>2</sup> and the volume 16 mm<sup>3</sup>. If we now continue doubling the length until the grain is 64 mm in length, or 32 times as long as the original, the area is 2048 mm<sup>2</sup> and the volume is  $6.5 \times 10^4$  mm<sup>3</sup>. The problem then is, which is the best measure of grain size? Do we say the grain is 32 times larger, or thirty thousand times larger? Because the force is proportional to the volume, we should regard the larger grain as being thirty thousand times larger than the original. This does not mean that Gibb's presentation is incorrect, but it does suggest that caution should be used when interpreting such graphs, Variation in average grain length does not give a true measure of the volume variation and therefore misrepresents--what we might call the mechanical size of the grains, an important boundary condition in any genetic discussion.

The purpose of the present study is to provide a more accurate representation of the grain size distribution (from thin sections) by directly measuring the area of each grain and then calculating the volume. Over 7,000 individual measurements were made on selected samples across the intrusion. Details of the analysis may be found in Appendix A. The results are presented in Figs. 7, 8 and 9. The variations in class interval provide three degrees of resolution of the grain size variation. The average grain size (in area) and the corresponding volume (see Appendix for method of calculation) are shown in Fig. 10,

Fig. 6 LENGTH, AREA, VOLUME RELATIONS



and the first and second order modes (the first and second highest modal frequency) in Fig. 11.

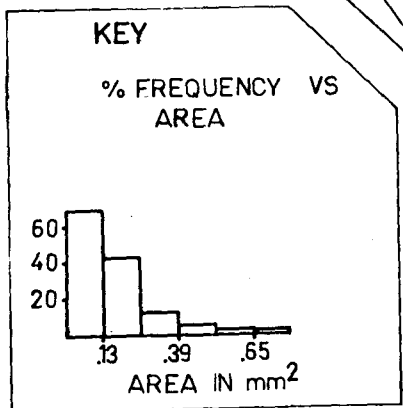
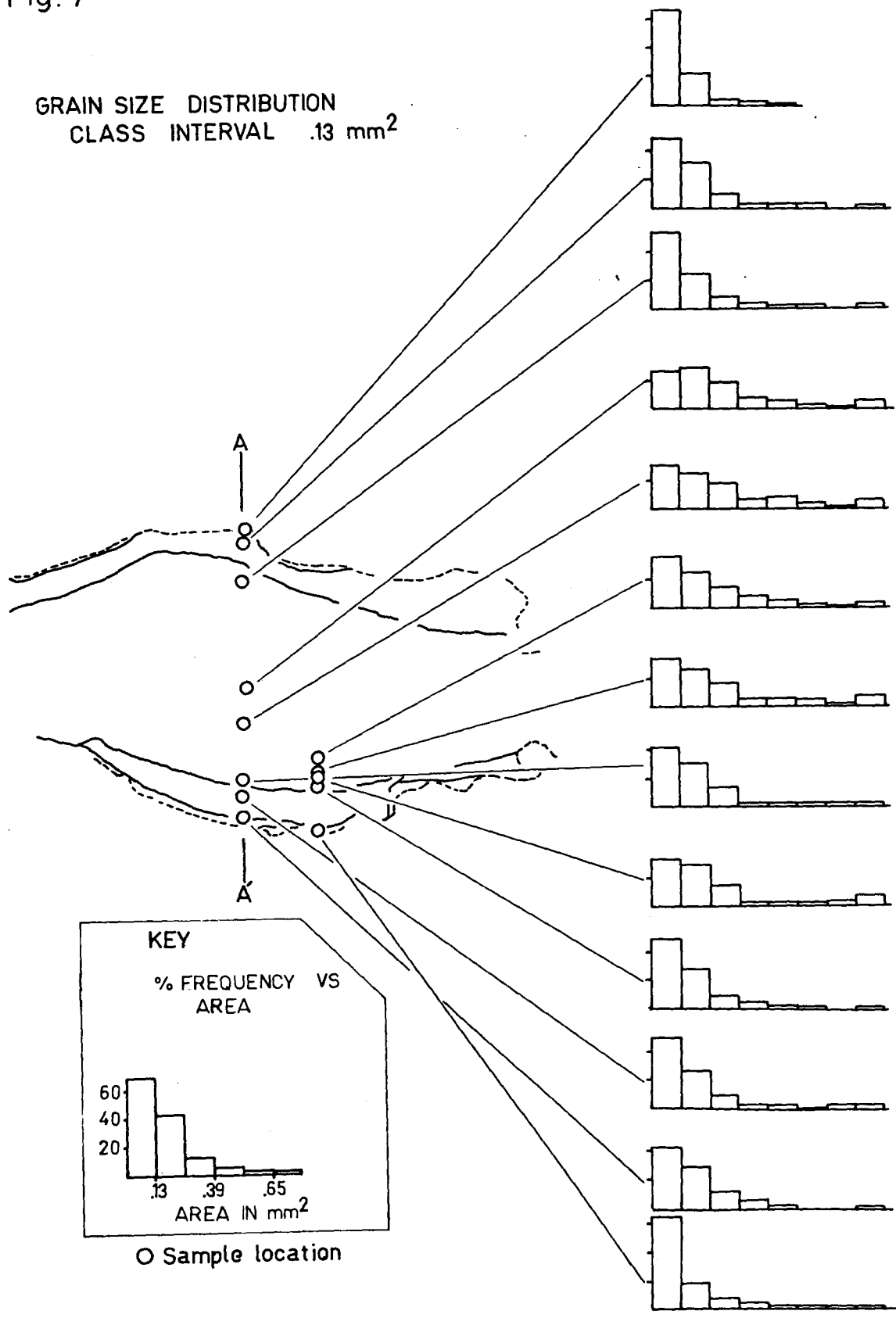
The M-factor or Maximum size factor for each location is shown in Figs. 12, 13, 14. This is a technique often employed by sedimentologists which is based on the simple idea that a sand body with several large stones is fundamentally different from one which contains small stones or no stones at all, i.e., the original transport energy may have been different or no large stones were available.

The same idea has been used here to represent the average size of the largest 10, 30 and 50 grains in each sample.

**See Appendix B, part D , for sample number location.**

Fig. 7

GRAIN SIZE DISTRIBUTION  
CLASS INTERVAL .13 mm<sup>2</sup>



○ Sample location

Fig. 8

### GRAIN SIZE DISTRIBUTION

CLASS INTERVAL  $.065 \text{ mm}^2$

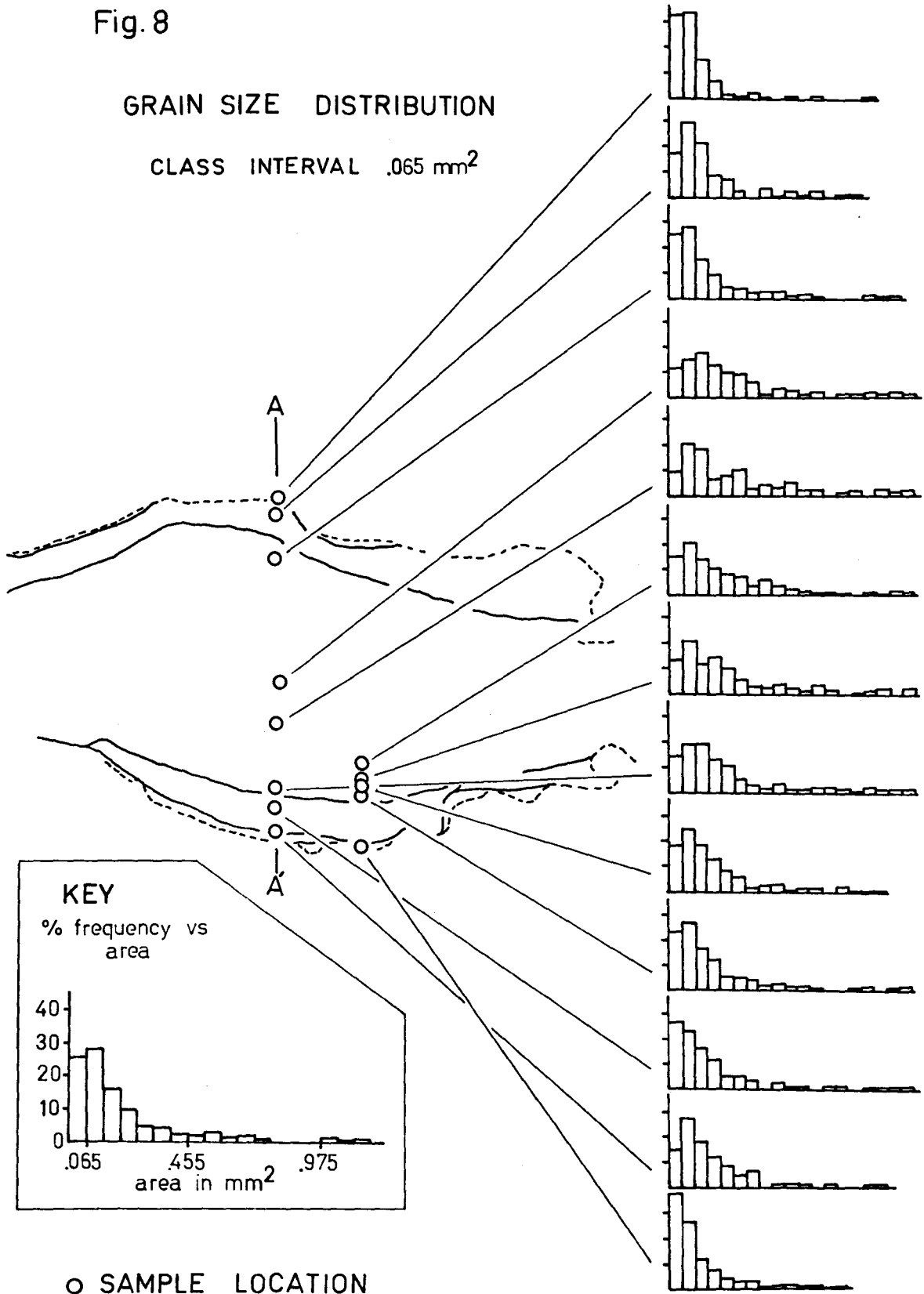
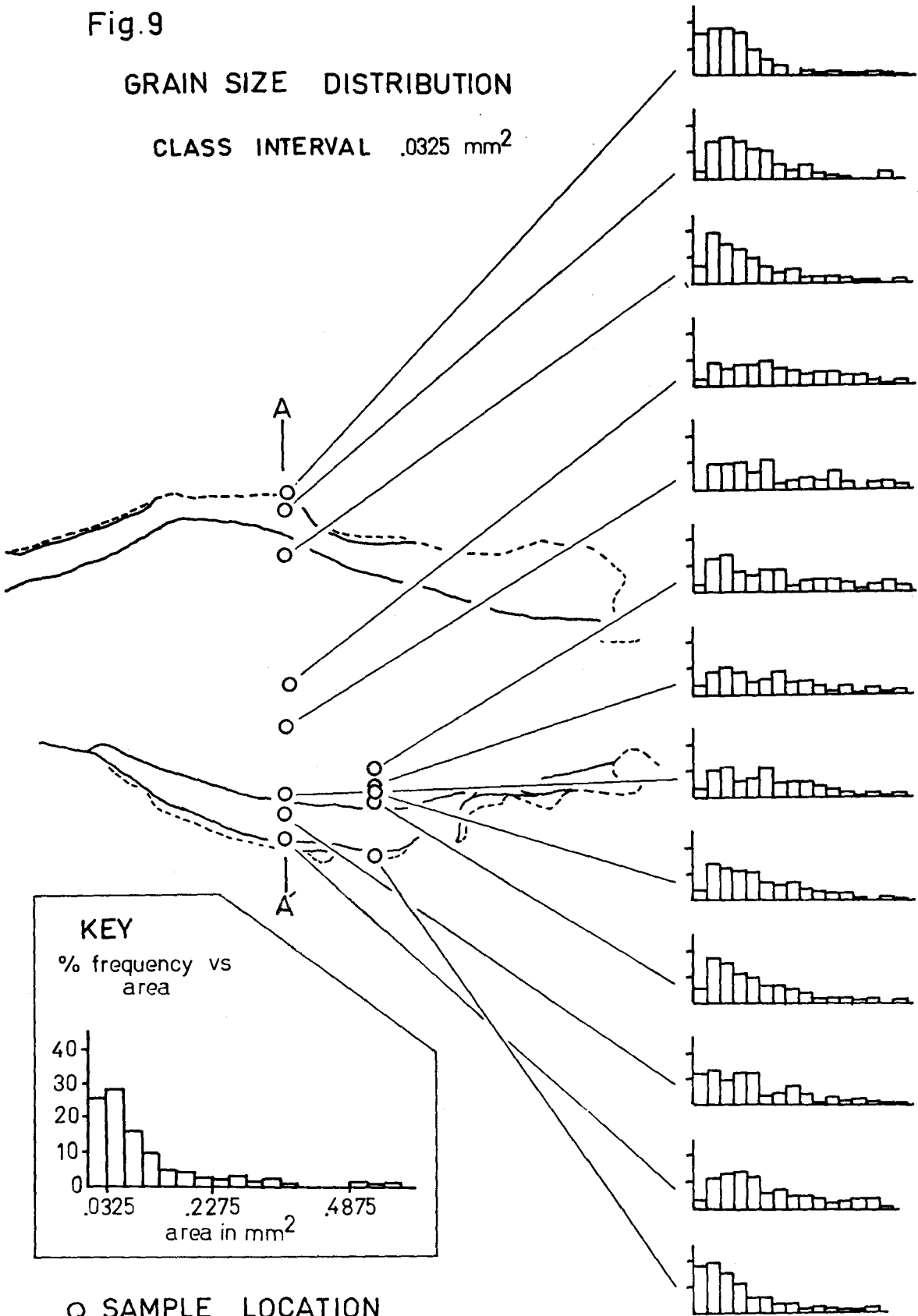


Fig.9

GRAIN SIZE DISTRIBUTION

CLASS INTERVAL  $.0325 \text{ mm}^2$



○ SAMPLE LOCATION

Fig.10 Average Grain Area and Volume

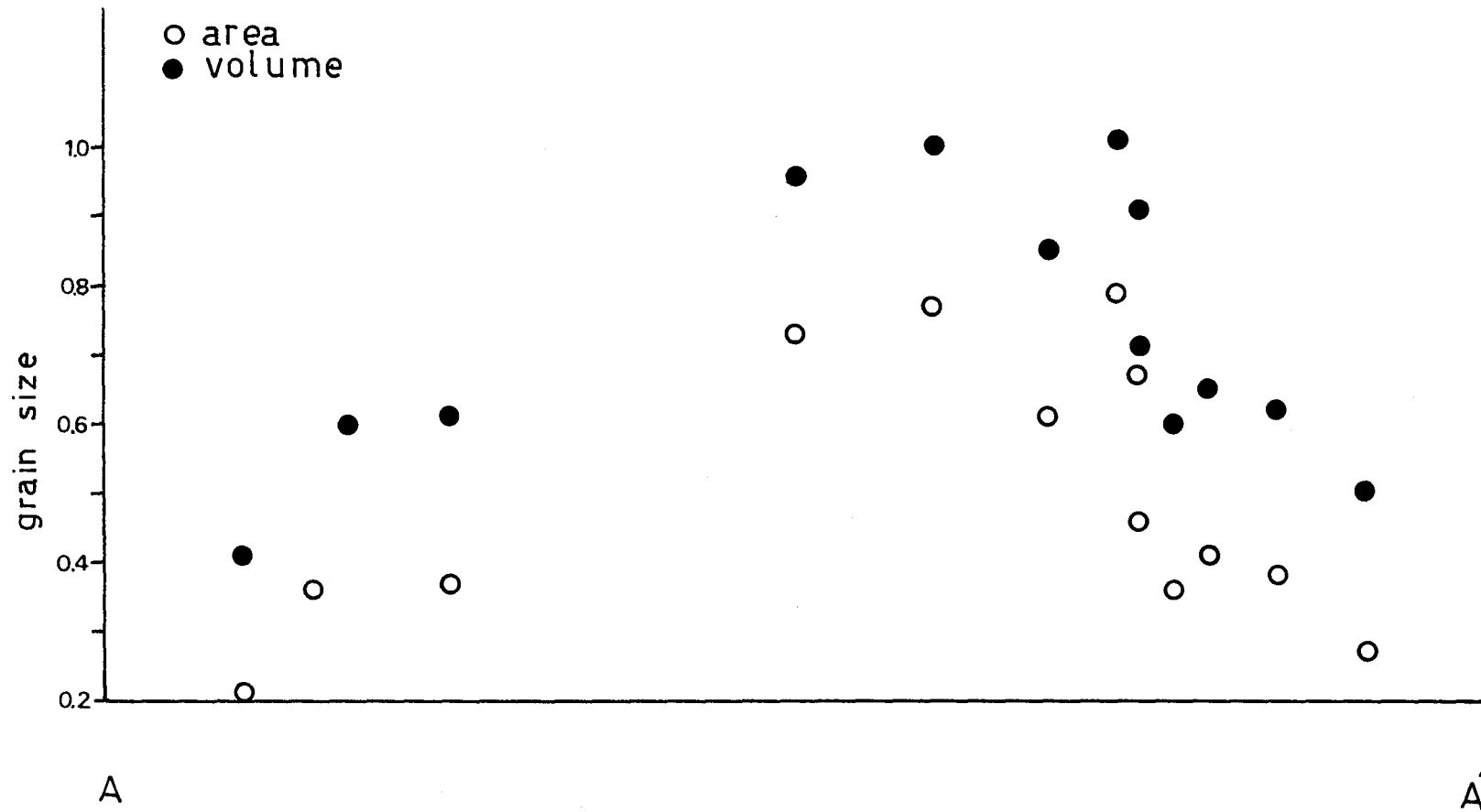


Fig.11 HISTOGRAM MODAL VALUES

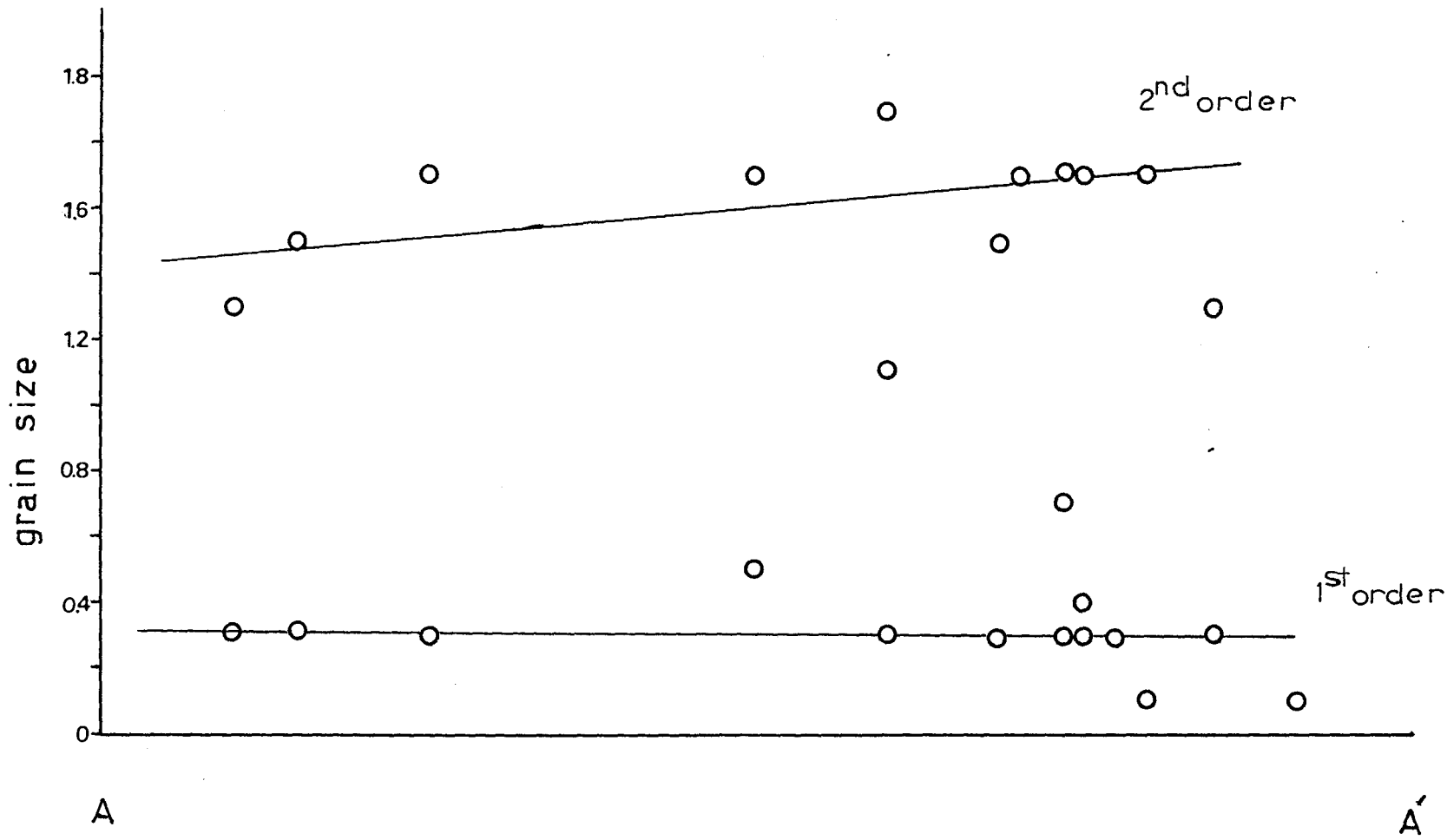


Fig. 12 M-FACTOR -10

Average Grain Area and Calculated Volume for the Largest 10 Grains from each measured section.

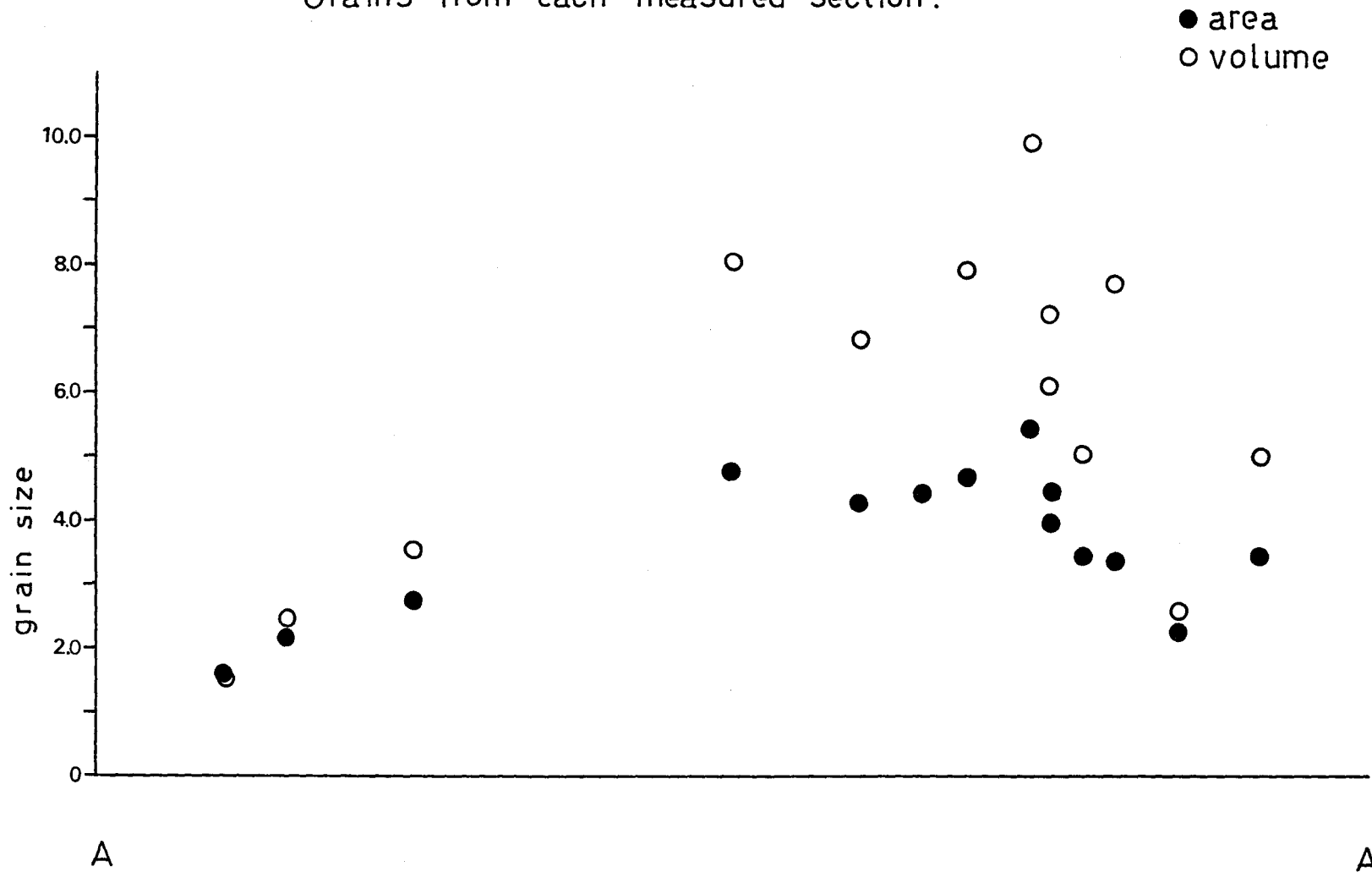


Fig. 13 M-FACTOR -30

Average Grain Area and Calculated Volume for the Largest 30 Grains from each measured section.

● area  
○ volume

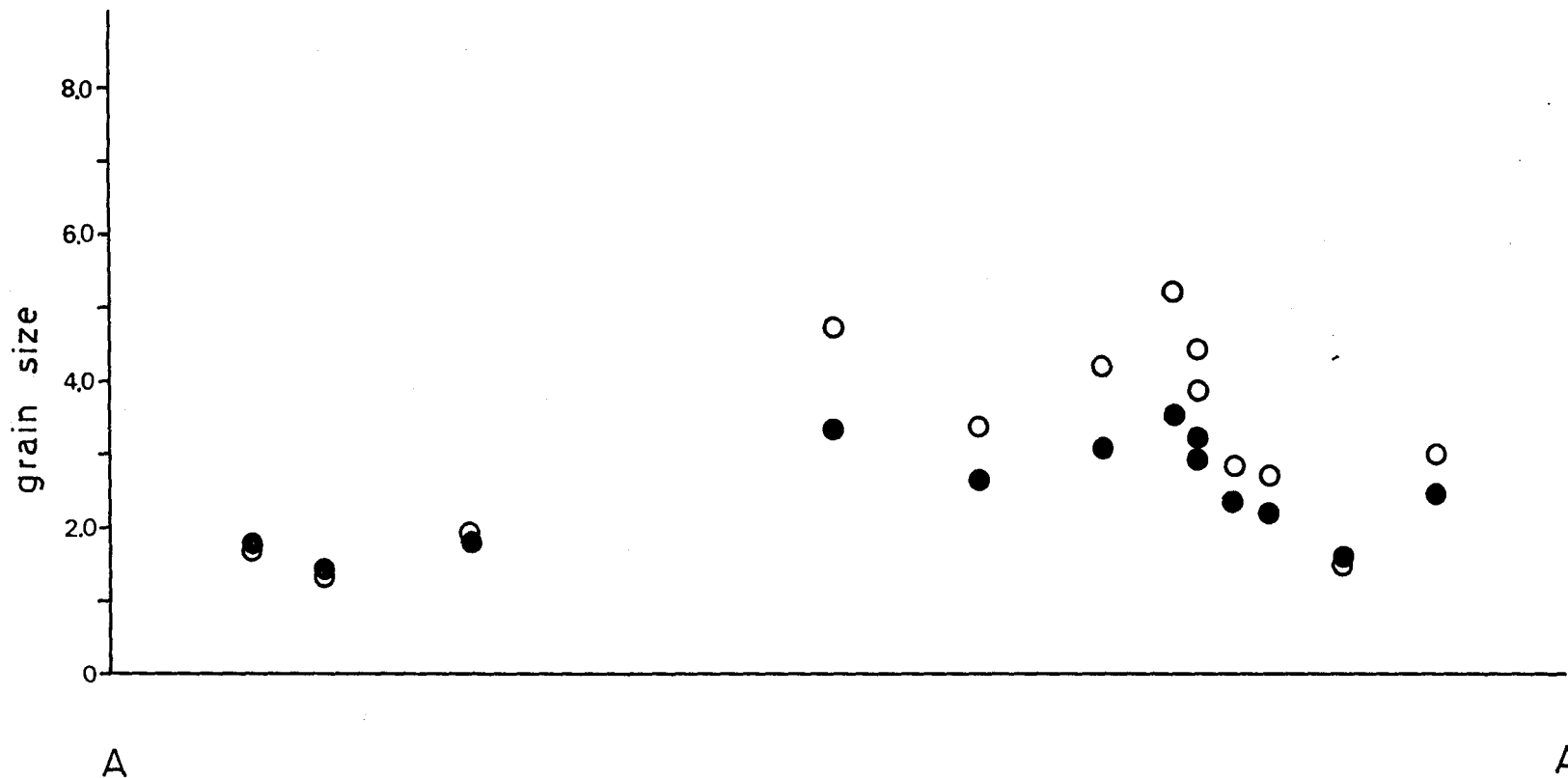
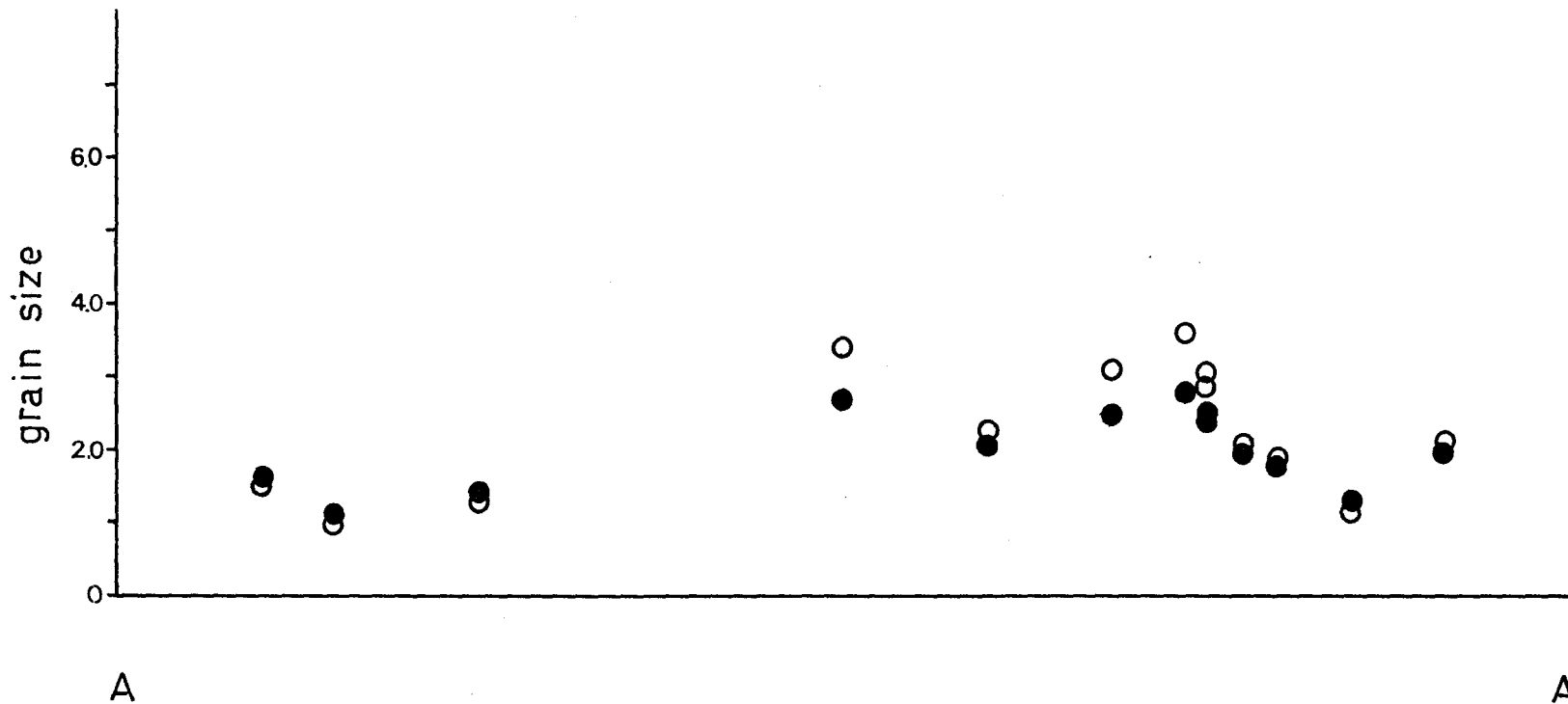


Fig.14 M-FACTOR -50

Average Grain Area and Calculated Volume for the Largest 50 Grains from each measured section.

● area  
○ volume



## ii) DISCUSSION AND RESULTS

The grain size distributions shown for three different class intervals all exhibit a similar pattern. Each is characterized by a shift in the frequency distribution toward the larger sizes, as well as a flattening of the distribution to include a larger range of sizes, as one moves from the margins toward the centre of the intrusion. This second observation is best demonstrated by the highest resolution distribution (class interval  $.0325 \text{ mm}^2$ ), which shows the distribution not only to be flatter, but also much more complex with greatly increased variability in proportions of grain sizes.

Fig. 10 shows the average grain area and calculated volume for each station plotted in their relative positions across the intrusion. Once again there is a central increase, however it is clearly shifted to the south.

The M-factor (Figs. 11, 12 and 13) shows a similar pattern to Fig. 10 (average area and volume). There is a gradual increase in the size of the largest grains until sample 110 is reached, after which there is a rather rapid decline back to sizes similar to the opposite edge of the intrusion.

To summarize, each of the above graphic methods indicate that the grains increase in size and variability toward the centre of the intrusion reaching a maximum value skewed somewhat to the south of the centre of the intrusion. Interestingly enough, this position corresponds to the edge of the central dunite (or olivine rich) zone outlined during field mapping.

Fig. 11 depicts the 1st, 2nd (and in two cases the 3rd) order modal values for each of the separate stations plotted in their respective positions. There is a fairly good grouping of first and second order modes, possibly suggesting two separate stages of crystal growth. However, there are a variety of explanations for such a pattern and close examination of the histograms indicates these trends (especially the second order ones) to be rather weak. Consequently little can be concluded about this information.

## CHAPTER IV

### FLOWAGE DIFFERENTIATION

Flowage differentiation can be defined as a process capable of causing crystal and chemical fractionation in natural magmas, due to the inherent flow properties of the mixture.

Bowen (1928) strongly emphasized the role of flow in the emplacement of mafic and ultramafic rocks. Fahrig (1962) and Baragar (1967) have described ultramafic sills from the Labrador Trough, which exhibit mineral and chemical variations attributable to flow. Simkin (1967), Drever and Johnson (1967) and Gibb (1968) have made similar observations for ultrabasic intrusions in Scotland. Raudsepp (1974) has examined a metagabbro sill complex in N. W. Ontario which indicates possible differentiation by flow.

The Labrador sills are described by Fahrig (1962) as "exhibiting a striking megascopic zoning parallel to their borders". The sills are zoned into three recognizable rock types, which are gradational into each other. He concludes that the parent magma was intruded as a mush of olivine crystals in a gabbroic silicate liquid. Flow resulted in an increased liquid fraction toward the top and base of the sill, and a central concentration of crystals.

Observations on numerous ultrabasic sills and dikes in Scotland (Simkin, 1967; Drever and Johnson, 1967; Gibb, 1968) may be summarized as follows:

1. There is a general increase in the size and number of

olivine crystals away from the margins of the intrusions, where olivine is virtually absent, to the centre, where sizes and abundance are greatest.

2. The majority of the olivine crystals show a tendency toward idiomorphism and are considerably smaller than the "groundmass" crystals, often being poikilitically enclosed by them.

Most of these features are thought due to flow which induced differentiation of a crystal-rich fluid. Modification by gravity is considered to be significant in non-vertical intrusions. However, its quantitative effect is unknown.

The process of flowage differentiation was first studied by Bhattacharji and Smith (1964) via quasiscale model experiments. They were attempting to explain the mineralogical features of the Muskox feeder dike (Northwest Territories, Canada), which is zoned parallel to vertical walls, with no chilled contacts between zones. The mineralogical symmetry (of the dike) precludes random injection of separate magmas, even at high temperature. They scaled their models using various oils and plastic particles to simulate a crystal-laden magma. Dynamic similarity was ensured by equality of Reynold's number between the model and the original body. Bhattacharji (1966, 1967), using similar scaling techniques, studied magmatic flow differentiation in sills. The scale models covered a range representing sills from 1.5 to 600 metres in width and apparent magma viscosities from 100 to  $3 \times 10^4$  poises, with an average apparent viscosity of  $3 \times 10^3$  poises.

Bhattacharji noted several basic problems inherent in such scaling. Since magma apparent viscosity and flow velocity vary greatly during intrusion in nature, absolute scaling is not possible. Also, the absolute equivalence of the force of gravity for the model and the original imposes a restriction which is impossible to circumvent in these experiments. Another drawback is that realistic estimation of the time duration of flow during intrusion has not yet been possible. The importance of these unknown boundary conditions will be discussed later.

Assuming, for the present, that the above restrictions are not critical to the final outcome, the pertinent observations made in these studies may be summarized as follows:

1. In laminar flow, the solid particles move away from the walls and gradually increase in concentration towards the centre.
2. Particles rotate as they move.
3. The rate of concentration toward the centre increases with velocity or shear gradient. Thus increasing concentration accelerates the process.
4. The rate of inward movement increases with particle size.
5. The establishment of the Poiseuille (parabolic) regime of flow in the non-Newtonian viscous mush can be inferred from the central plug.
6. Zoning can be disturbed (particularly in sills) due to fluctuations of the velocity-pressure relation

in the melt, gravity settling, and strong pulsating flow conditions.

Based on the above observations, Bhattacharji has concluded that the flow of magma in the presence of a boundary results in forces sufficiently strong even at low magma velocity to produce crystal segregation from the walls and inward migration of the crystals toward the conduit centre. He considers the wall effect, due to the mechanical interactions of particles and rigid walls, and the Magnus effect, arising from a combination of rotatory and translatory motion of a particle relative to the undisturbed flow of the fluid, to provide satisfactory fluid dynamic explanations for such size sorting during flowage. He also notes that the volume concentration of crystals in the crystal-melt mush is critical in determining the nature of the differentiation.

Komar (1972a) has reviewed the forces acting on single spheres in a fluid (the Magnus and wall effect) and concludes that it is doubtful whether these forces play any significant role in phenocryst migration. Using semi-empirical equations for grain dispersive pressure (the pressure due to mechanical interactions between phenocrysts) developed by Bagnold (1954), he found fairly good agreement between calculated phenocryst distributions and those observed in the field (Komar 1972a,b).

When a suspension of grains and fluids is sheared, the interaction results in mutual repulsion of grains or a "dispersive grain pressure". No collision between grains is necessary, although it may occur. Bagnold first investigated the idea of grain dispersive pressure and defined the "Bagnold number" or dimensionless shear stress number:

$$B = \frac{\text{inertia stress}}{\text{viscous stress}} = \frac{f_s}{\eta} \Lambda^{1/2} D^2 \left( \frac{dU}{dy} \right) \quad (1)$$

where:

$\Lambda$  is the linear concentration defined by

$$\Lambda = \frac{1}{\left( \frac{C_0}{C} \right)^{1/3} - 1} \quad (2)$$

$C_0$  = the maximum possible concentration;

equal to 0.74 for tightly packed uniform spheres;

and 0.65 for many natural grain mixtures;

$C$  = volume concentration of solid particles;

$\rho_s$  = density of the solid phenocrysts;

$\eta$  = viscosity of the fluid portion of the solid  
fluid suspension (in poise, assumed to be Newtonian)

$D$  = particle diameter;

$\frac{dU}{dy}$  = rate of shear.

For uniform spherical grains, the nature of the grain interactions vary as follows:

$B < 40$  - grain-viscous region; viscous effects of the fluid prevail;

$B=40-400$  - region of transition;

$B > 400$  - grain-inertia region--the inertia of the grains dominates the viscosity completely.

The value of the grain dispersive pressure,  $P$ , is given by the expressions:

$$\text{for } B < 40 \quad \Lambda > 2.5 \quad P_v = a_v \Lambda^{3/2} \eta \frac{dU}{dy} \quad a_v = \text{constant} \quad (3)$$

$$\Lambda < 2.5 \quad P_v = 1.3 (1+\Lambda) \left(1 + \frac{1}{2}\Lambda\right) \eta \frac{dU}{dy} \quad (4)$$

$$\text{for } B > 400 \quad P_i = a_i \rho_s (\Lambda D)^2 \left(\frac{dU}{dy}\right)^2 \quad a_i = \text{constant} \quad (5)$$

Note that in the grain-inertia region, the grain dispersive pressure is directly proportional to the size (squared) and density of the particles. This is one possible explanation for the size sorting effect which is observed to occur in experiments and natural samples.

The velocity profile of the intruding magma is dependent on its rheological character, and will vary from parabolic (for a Newtonian fluid) to plug-like (for a non-Newtonian fluid). The velocity gradient is given by:

$$\frac{dU}{dy} = -U_m \left(\frac{3n+1}{n}\right) \frac{y^{2/n}}{Y^{(n+1)/n}} \quad (6)$$

where:

$U_m$  = the mean velocity;

$n$  = a measure of the degree of non-Newtonian behaviour;

the smaller the value of  $n$ , the greater the departure from Newtonian character;

$y$  = coordinate axis across the sill (varies from  $-y$  to  $+y$ );

$Y$  =  $1/2$  width of sill.

The velocity gradient increases from 0 at  $y = Y$  to a maximum at  $y = 0$ ; the grain dispersive pressure  $P$  varies accordingly. This gradient

of dispersive pressure will cause particles to migrate towards the centre of the dike. Migration will continue until the grain dispersive pressure is constant across the dike ( $P_u = \text{constant}$ ). This equilibrium condition can be used to calculate concentration profiles for various initial conditions (Fig. 15). Komar (1972) has noted that comparison of the calculated distributions with natural concentration profiles indicate a value of  $n$  in the order of 0.1 to 0.2. However, he points out that natural magmas generally do not show such strong non-Newtonian behaviour, and suggests that possibly a balance exists between the viscous dissipation forces and the pressure gradient causing the flow. This is thought to be due to the effective viscosity increase resulting from increased concentration away from the wall.

The analysis is modified to include this consideration by solving the Navier-Stokes equations for fluid motion with equation (3) and assuming the Roscoe (1952) formula for apparent viscosity. The form of the solution is strongly dependent on the relation for the apparent viscosity, but in general it is non-Newtonian and can best be described as plug flow. The plug has an average velocity close to the maximum, with a rapid decrease toward the wall where  $U = 0$ . It should be noted that this solution gives distributions similar to natural ones without assuming strong non-Newtonian behaviour. An example of the velocity, shear stress and concentration profile for one particular total concentration is shown in fig. 16. Concentration profiles for varying total concentrations (the total number of grains) are illustrated in Fig. 17.

Fig.15 Crystal Concentration for Various Fluids of Increasing Non-Newtonian Character after Komar 1972a

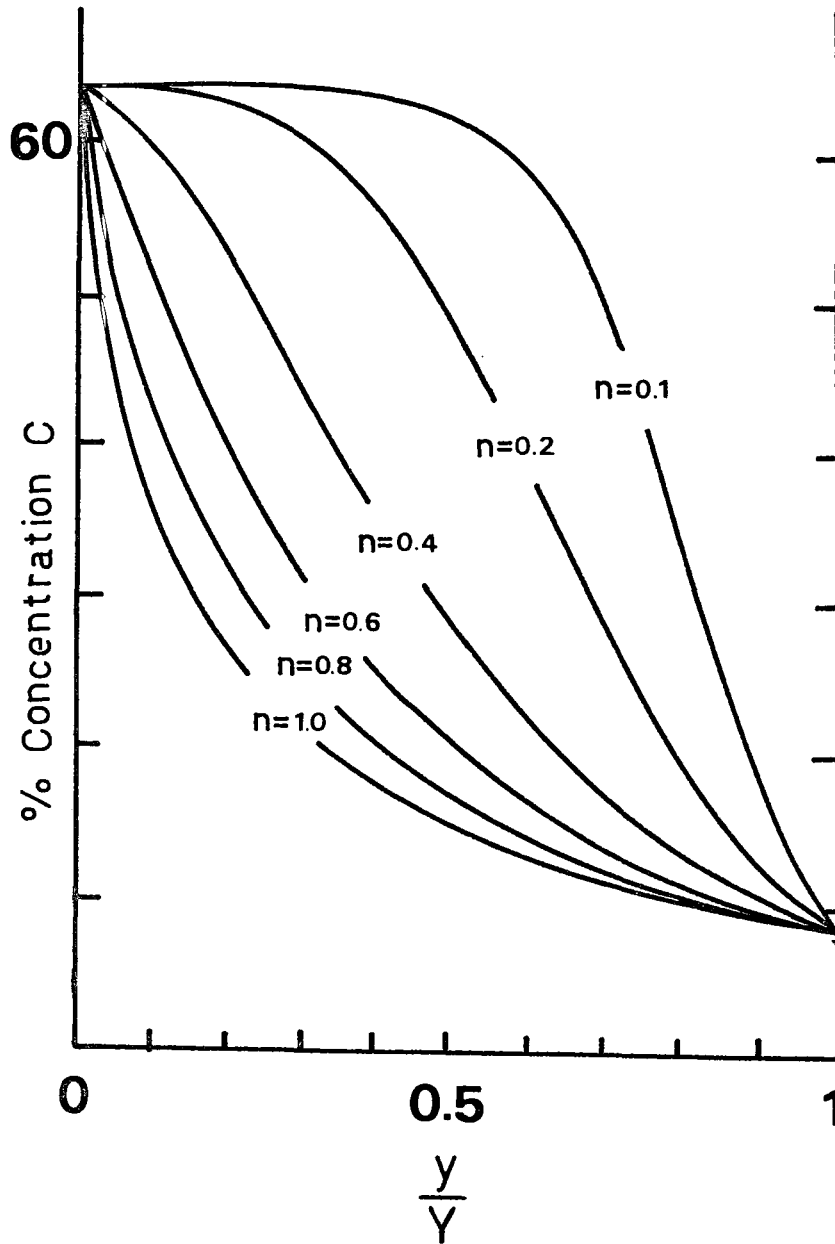


Fig.16 Crystal Concentration, Shear Stress and Velocity Profile for a Wall Concentration of 10% and a Max. Vel. of  $U$  . after Komar 1972a

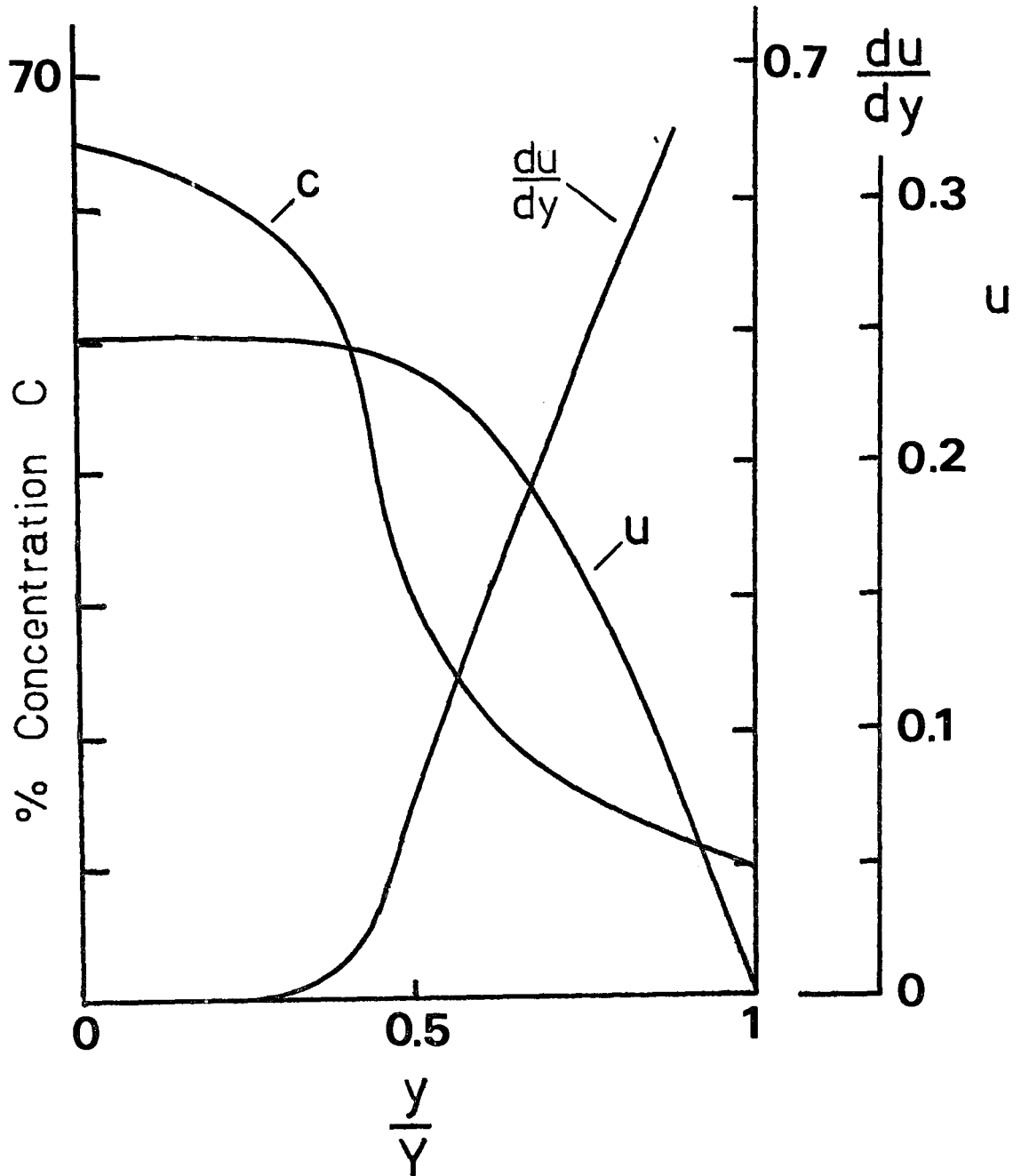
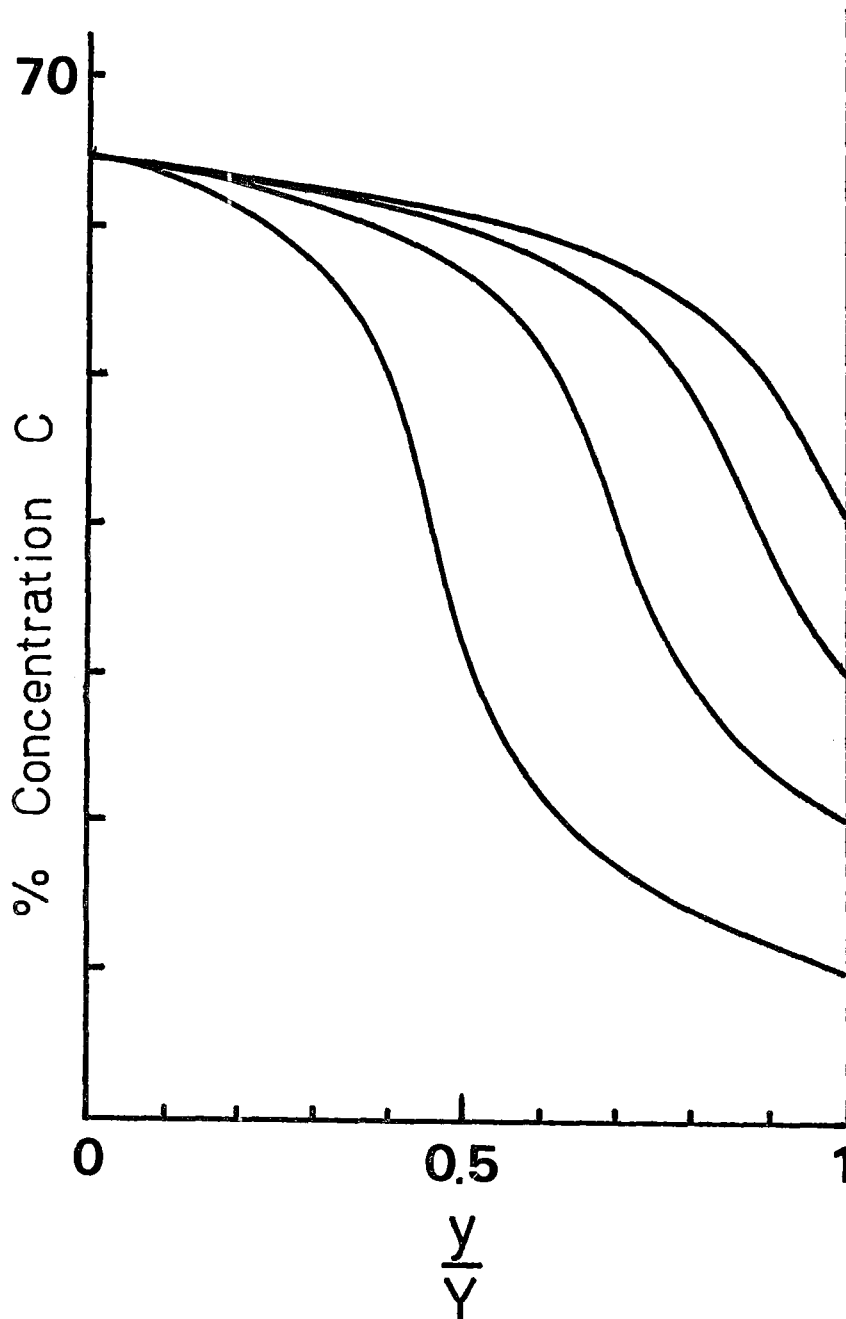


Fig.17 Crystal Concentrations for Various  
Wall Concentrations (see text)  
(assuming modified analysis) after Komar 1972a



Asymmetric distributions may occur in two ways: sorting during intrusion due to downward forces and settling of phenocrysts following intrusion, both due to gravity. Komar (1972a) did not include the effect of gravity in his analysis, but he did discuss how it may modify the calculated distributions. The net gravitational force on a particle is given by:

$$F_g = \frac{\pi}{6} (\rho_s - \rho) g D^3 \quad (7)$$

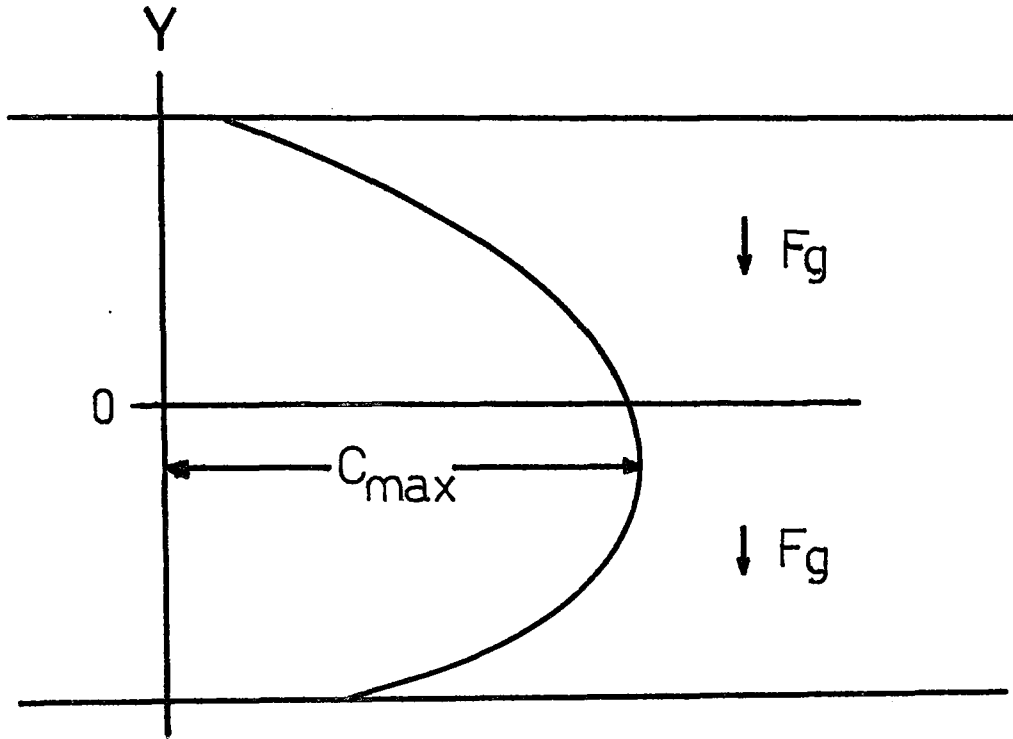
where:

$(\rho_s - \rho)$  = the density difference between the particles  
and the fluid.

$D$  = diameter of the particles.

Komar suggests that, during flow, an equilibrium is reached between the grain dispersive pressure and the downward force due to gravity. This results in a shift in the centre of the maximum concentration of the kind shown in Fig. (18). The resulting phenocryst distribution may be roughly approximated by superposition of the normal distribution due to grain dispersive pressure on the gravity profile.

Fig.18 Gravity Skewed Concentration Profile  
- after Komar 1972 a



## CHAPTER V

### A. DISCUSSION

The megascopic zoning exhibited by these sills is considered to be an important genetic feature. Although fig. 2 (Geology of Bravo Ultramafics) suggests definite borders exist between zones, field mapping indicates these borders to be completely gradational. Furthermore there is no field evidence of crystal settling or multiple intrusion. This is shown by continuous outcrop exposure in the field and is supported by the systematic chemical trends and continuous size and modal variation of original olivine. This evidence precludes the possibility of multiple intrusion. Thus we are faced with the conclusion that the initial magma was a mafic liquid charged with a high concentration of olivine crystals, in which differentiation occurred by crystal segregation. Pyroxene crystallized later as evidenced by large interlocking crystals, poikilitically enclosing the olivine.

There are two important components to the differentiation:

1. the gross lithologic symmetry
2. the more subtle chemical and grain size asymmetry

The gross symmetry, as has been discussed above, is mineralogic in nature and is defined by the systematic increase in olivine from the border to the centre of the intrusion, corresponding to a complimentary decrease in pyroxene. This study has shown that, although the background olivine grain size distribution is relatively constant throughout the sill, there is a significant increase in the large sizes away from the

margins toward the centre. This central maximum is skewed southward, the largest sizes being near the south margin of the central olivine rich zone. The overall olivine distribution is shown schematically in fig. 19.

The chemical analyses directly reflect the mineralogic zoning, for example, the rapid increase in Mg toward the central zone corresponds to the original increase in olivine. It is interesting to note that Fe does not show this trend, indicating that the initial olivine was Mg rich. This conclusion is supported by Fahrig (1962) and Beall (1962) who report the olivine from similar intrusions to be in the range of chrysolite.  $N_s$  (nickel in sulfides) and S both show an increase toward the south of the central zone, corresponding to the position of the maximum olivine grain size.

Based on these observations I interpret the south side of the sill to be the stratigraphic base. Thus the sill was intruded in a horizontal (or sub-horizontal) position; the asymmetry being imposed by gravity. Supportive evidence for this conclusion comes from Beall (1962) and Robertson (1975) who have examined spatially associated sills of similar composition. These sills exhibit strong gravity differentiation as well as close proximity to bedded sediments and pillow lavas, each of which contain directional indicators in agreement with the top direction indicated by the sills. In addition, the majority of the sulfide ore bodies are at the south contact of the country rock with the intrusive and appear to have settled out of the initial melt.

Assuming that the above conclusion is correct, let us consider

# Schematic Representation of Original Olivine Distribution

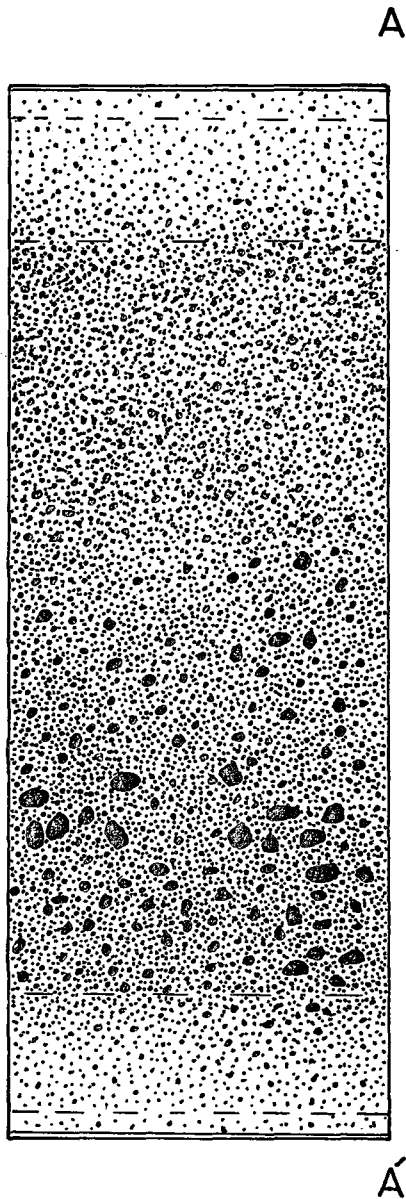
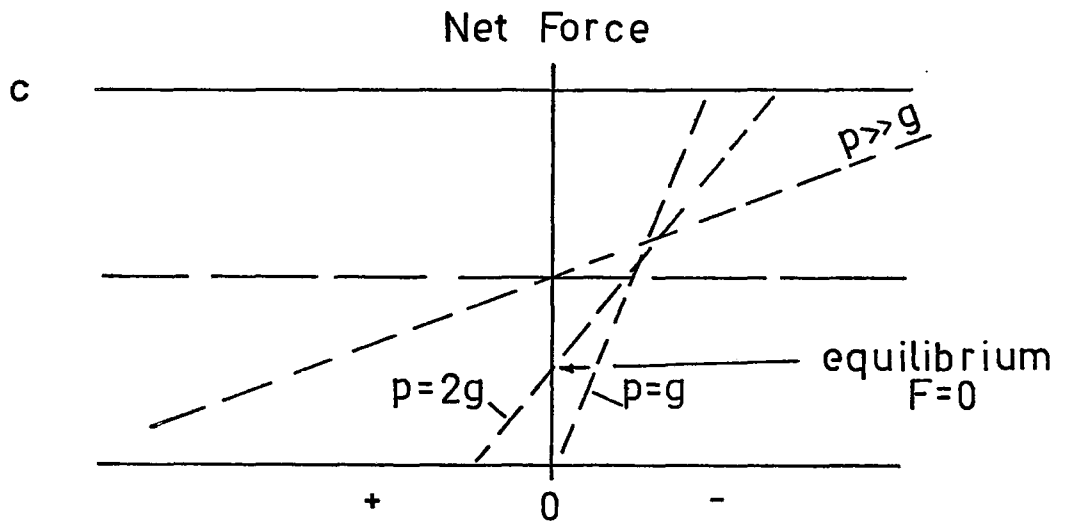
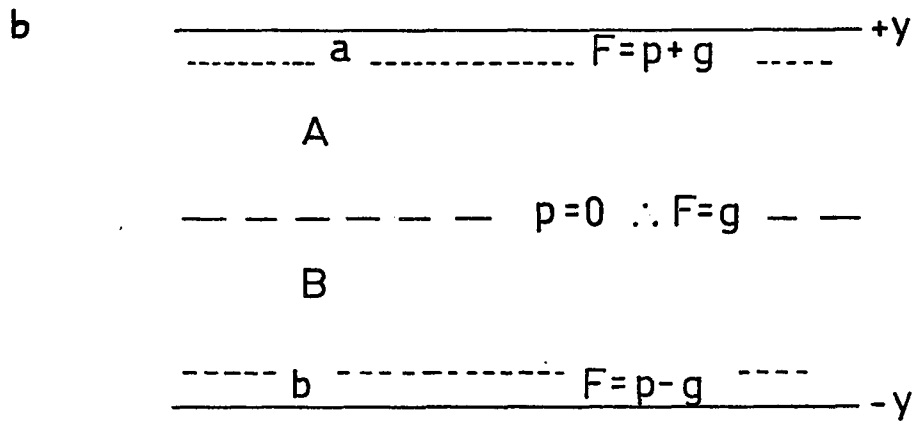
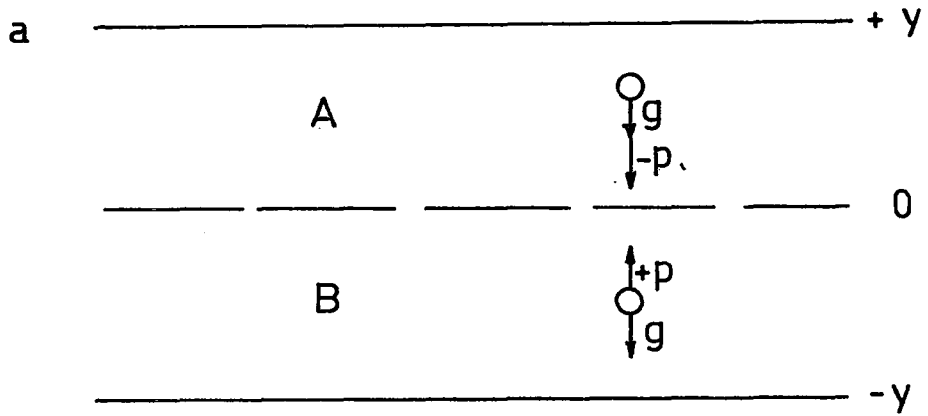


Fig. 19

the forces which act on a single particle during intrusion. We will approximate the geometry of the sill contacts to two infinite horizontal sheets. The forces considered important are gravity, which acts in a downward direction and is given a negative sign and grain dispersive pressure which may be either negative or positive. This hypothetical model is shown in fig. 20a. In the upper region (region A) the total force on a particle is  $g + p$ , as  $p$  and  $g$  are both negative, and in the lower region (region B) the total force is  $p - g$ . This is due to the fact that gravity acts downward in both cases. However, as discussed before, grain dispersive pressure acts in a direction away from the conduit walls toward the centre. Thus it changes sign from the upper region to the lower.

We may specify the relative values of  $p$  and  $g$  at each location by choice of suitable boundary conditions. This method is well explained by Johnson (1970) and is employed in a similar analysis by Gibb (1968). Consider fig. 20b. Field work and subsequent petrographic studies indicate that the olivine concentration in region b is low as compared with the central region. Therefore (assuming an initially homogeneous magma), we know that olivine did move toward the central region. Hence, in region b, grain dispersive pressure was greater than the gravitative force ie.  $p > g$  and therefore the net force is  $F = p - g$ , where  $F$  is positive. In region a the force must be  $p + g$  and greater than  $2g$ , as we have already shown that  $p < g$ . At  $y = 0$ , the centre of the sill,  $p = 0$  (there is no grain dispersive pressure), consequently the net force equals  $g$  and is negative. To summarize, the net force changes from a

Fig. 20 FORCE DISTRIBUTION  
 (g=gravity , p=grain dispersive pressure)



negative to a positive quantity between  $-y$  and  $y = 0$ , and therefore passes through zero. The position at which the force passes through zero marks the equilibrium position of any given particle.

Fig. 20c shows the net force for various values of  $p$  and  $g$  using the relative values we have determined as boundary conditions or limits. The line shown  $p = g$  is an extreme value as  $p$  cannot be less than  $g$ . This places the equilibrium position of any given grain at the bottom contact of the sill. A value of  $p = 2g$  places the equilibrium position approximately half way between the contact and the centre. In general as  $p$  increases the equilibrium position edges closer to the centre, reaching a limit at  $p = \infty$  at which point the net force line becomes horizontal.

The analysis to this point indicates that all of the olivine grains should have moved to a position somewhere in region B where the force of gravity is balanced by the grain dispersive pressure. This would occur even if  $p$  is much greater than  $g$  as the grains would still only be in equilibrium below the centre line. Field evidence indicates that this is not the case. The approach we have taken is inherently wrong, in that the value of the grain dispersive pressure is directly dependent on the concentration of grains and we have only considered a single grain.

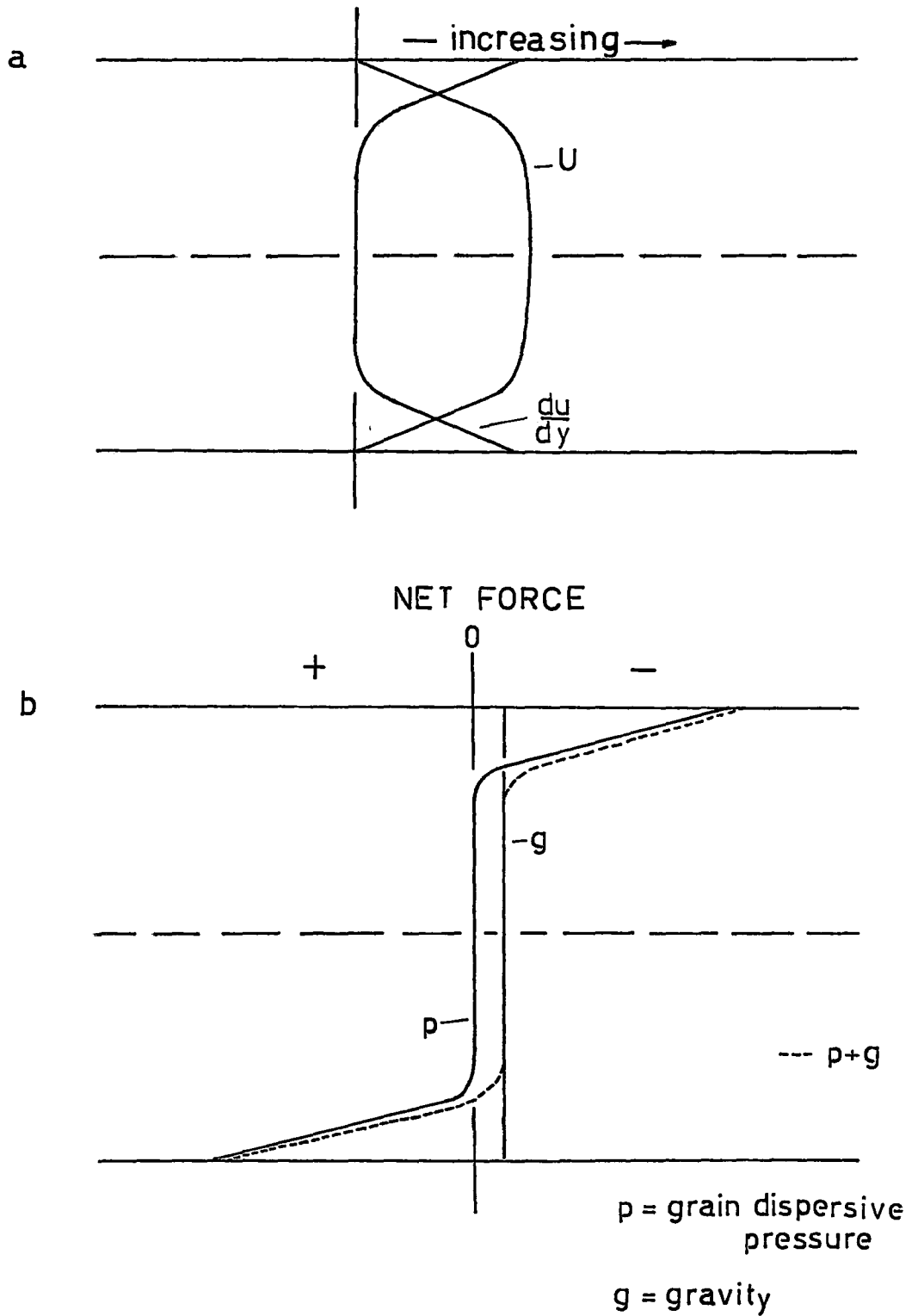
To achieve a more realistic model we must consider the character of the suspension. The modal concentration of olivine determined by point counting ranges from less than 10% at the margins to 75% in the central region, with a large portion in the range 70—75%. Such high

concentrations have a marked effect on the apparent viscosity of the suspension as well as the flow behaviour and are best thought of as non-Newtonian (Johnson 1970) (Shaw 1965,1969). At low flow velocities such suspensions commonly approximate to Bingham fluids. This is a fluid which has a shear strength, in other words a certain shear stress must be exceeded before flow takes place. Once flow is initiated the constant of proportionality (or Bingham viscosity) between shear stress and the rate of shear strain is a linear one (analogous to Newtonian viscosity). The velocity profile (or flow curve) of Bingham fluids is characterized by a rapid increase in velocity from the margin toward the centre, where a plug of fluid is moving with a constant velocity close to the maximum. The shear rate shows exactly the opposite trend, having a maximum near the border and decreasing to a value close to zero for the central plug. It follows from equations 3, 4, and 5 (CHAPTER IV) that under given conditions during plug flow, the grain dispersive pressure will follow a similar pattern to the shear rate. Hence grains in the marginal regions will be forced toward the central zone and become part of the flowing plug. The extent to which this inward migration will take place is governed by the initial average concentration (for a given flow rate) as indicated by equations 3, 4, and 5. An example of these conditions has already been illustrated in Figs. 16 and 17. The velocity profile ( $U$ ) and corresponding rate of shear stress ( $\frac{du}{dy}$ ) for a flowing plug is shown in fig. 21a. Grain dispersive pressure is directly proportional to shear rate, therefore it will have a relatively high value near the margins decreasing to almost zero within the plug. The

Fig. 21

# FORCE DISTRIBUTION

within Bingham Fluid



net force at each location within the sill is shown in fig. 21b (dotted line). This is the resultant produced by vector addition of  $p$  and  $g$ . An arbitrary (maximum) value of  $p$  approximately one order of magnitude larger than  $g$  has been chosen. This is based on the observation that the intrusion studied shows a maximum grain concentration (in terms of packing) within the central plug and a considerably low value for the margins. Thus, it would appear the process was fairly efficient. It should also be noted that, the larger  $p$  becomes with respect to  $g$ , the more symmetric the mineral zoning becomes. On a field scale the Bravo sills are symmetric. Fig. 21b also indicates that within the central plug, gravity is the dominant force and therefore the net force is negative. This will result in a size sorting within the plug during flow, ie. the larger and/or denser minerals will make their way to the stratigraphic base of the plug.

## B. SUMMARY AND CONCLUSIONS

This grain size analysis employed in this thesis clearly demonstrates the subtle complexities of the olivine grain size distribution found within the Bravo ultramafic sills. To summarize, the analysis indicates that the average olivine grain size (as well as the average size of the largest grains) increases as one moves away from the sill contact toward the centre of the intrusion. That this is also the pattern of maximum olivine concentration, is indicated by point counting determination of modal olivine and field observations. Further, the analysis indicates the distribution to be skewed southward, the largest grains being close to the south edge of the central olivine rich zone.

Consideration of the above distribution allows determination of the relative boundary conditions within the confines of a sheet intrusion, assuming grain dispersive pressure and gravity to be the two predominant forces. The resultant force distribution indicates that all the olivine crystals should have moved to a position of equilibrium close to the south side of the central olivine rich zone. As this is clearly not the case, the analysis is modified by considering the rheologic character of the crystal-liquid suspension as a whole. It is concluded that the magma can best be thought of as a Bingham fluid.

The known shear stress distribution associated with the central flowing plug of a Bingham fluid allows accurate determination of the grain dispersive pressure and hence determination of the net force distribution through vector addition of the grain dispersive pressure with the force of gravity. The final net force distribution indicates

that along the margins of the intrusion grain dispersive pressure is the predominant force; olivine grains being forced toward the centre of the intrusion from both sides. However, within the central plug grain dispersive pressure is negligible and the force of gravity is free to produce the size sorting of crystals observed.'

From an economic point of view it is interesting to note that the maximum concentration of  $Ni_s$  (Nickel in sulfides) coincides with the position of the maximum olivine grain size. It would appear that the sulfide blebs suspended in the melt were subject to the same force distribution as the olivine crystals and consequently were concentrated in the same area. Conversely, large concentrations of sulfide are found close to the edge (base) of the intrusion, commonly in structural pockets. This suggests that the sulfide blebs are held in suspension only up until some threshold size is reached after which they sink to the base of the intrusion where they are carried along by the flow, eventually being trapped in structural lows.

It is concluded that the Bravo Ultramafic sills developed their mineral and chemical zoning as a result of Flowage Differentiation.

REFERENCES

- Bagnold, R.A., 1954. Experiments on a gravity-free dispersion of large solid spheres in a Newtonian fluid under: Royal Soc., London, Proc, ser. A. v.225 p.49-63.
- Baragar, W.R.A., 1974. Preliminary report on volcanic studies in the Cape Smith-Wakeham Bay belt, New Quebec; Geol. Sur. Can. paper 74-1, Part A.
- Baragar, W.R.A., 1967. Wakuack Lake map-area, Quebec Labrador; Geol. Surv. Canada, Mem 344.
- Barriere, M., 1976. Flowage Differentiation: Limitation of the "Bagnold Effect" to the Narrow Intrusions, Mineralogy and Petrology, 1976.
- Beall, G.H., 1959. Cross Lake area, New Quebec; Quebec Dept. Mines, Prelim. Rept. 396.
- Beall, G.H., 1960. Laflamme Lake area, New Quebec, Quebec Dept. Mines, Prelim. Rept. 435.
- Beall, G.H., 1962. Differentiation controls in subsiliceous Gabbros. Unpubl. PHD. Thesis, Mass. Inst. Tech. 271 p.
- Bergeron, R., 1959. Povungnituk Range area, New Quebec; Quebec Dept. Mines, Prelim. Rept. 392.
- Bhattacharji, S., 1964. Fluid mechanics model for the mechanics of differentiation of basaltic magma during flowage: Geol. Soc. America Spec. Paper 76 p.14-15 (Abst.).

- Bhattacharji, S., 1966. Experimental scale model studies on flowage differentiation in sills; Geol. Soc. America Spec. Paper, 87.
- Bhattacharji, S., 1967. Mechanics of flow differentiation in Ultramafic and mafic sills; S. Geol. 75, p.101-112.
- Bhattacharji, S. and Smith, C.H., 1964. Flowage differentiation. Science, V.145, p.148-174.
- Bottinga, Y. and Weill, D.F., 1972. The Viscosity of Magmatic Silicate Liquids: A Model for Calculation. Am. Jour. Sci. vol. 272, p.438-475.
- Bowen, N.L., 1928. The evolution of the Igneous Rocks: Princeton, New Jersey, Princeton Univ. Press, 332 p.
- Davidson, A., 1972. The Churchill Province, in variations in Tectonic Styles in Canada, Price, R.A. and Douglas, R.S. (eds), Geol. Assoc. Can. Spec. Pap. No. 11, p.381-433.
- Dimroth, E., Baragar, W.R.A., Bergeron, R., and Jackson, G.D., 1970. The filling of the Circum-Ungava Geosyncline; in Baer, A.S. (ed.). Basins and geosynclines of the Canadian Shield; Geol. Surv. Can., Paper 70-40, p.45-142.
- Drever, H.J. and Johnston, R., 1967. Picritic Minor Intrusions, in Wyllie, F.S. ed., (as above).
- Fahrig, W.F., 1962. Petrology and geochemistry of the Griffis Lake ultra basic sill of the Central Labrador trough; Quebec; Geol. Surv. Can. Bull. v.77, p.1-39.

- Frangipane, M. and Schmid, R., 1974. Point counting and its Errors; A Review. Schweig. Min. Petr. Mitt., 54, p.19-31.
- Friedman, G.M., 1958. Determination of sieve-size distribution from thin-section data for sedimentary petrological studies, Jour. Geol. Vol. 66, p.394-416.
- Gelinas, L., 1962. Watts Lake area, New Quebec; Quebec; Dept. Nat. Res., Prelim. Rept. 471.
- Gibb, F.G.F., 1968, Flow differentiation in the Xenolithic ultrabasic cykes of the Cuillins and Strathaird Peninsula, Isle of Skye, Scotland: J. Geol. Soc., 9, p.411-443.
- Goldsmith, H.L. and Mason, S.G., 1961. Axial migration of Particals in Poiseuille flow: Nature v. 190, p.1095-1096.
- Jaeger, J.C., 1957. The temperature in the neighbourhood of a cooling intrusive sheet: Am. Jour. Sci., v.255, p.306-318.
- Johnson, A.M., 1970. Physical Processes in Geology. Freeman, Cooper and Company, 577 pp.
- Johnson, A.M. and Pollard, D.D., 1973. Mechanics of Growth of some Laccolithic Intrusions in the Henry Mountains, Utah I. Tectonophysics. 18.
- Komar, P.D., 1972a. Mechanical interactions of phenocrysts and the flow differentiation of igneous dikes and sills: Geol. Soc. America Bull., v.83, no.4, p.973-988.
- Komar, P.D., 1972b, Flow Differentiation in Igneous Dikes and Sills: Profiles of velocity and Phenocryst Concentration: Geol. Soc. America Bull. v.83, pg. 3443-3448.

- Murase, T. and McBirney, A., 1973. Properties of some Common Igneous Rocks and their Melts at High Temperatures. Geol. Soc. Amer. Bull. v.84, p.3563-3592.
- Naldrett, A.J., 1973. Nickel Sulphide Deposits--Their Classification and Genesis, With Special Emphasis on Deposits of Volcanic Association. CIM Bull. p.45-63.
- Pollard, D.D., 1973. Derivation and Evaluation of a Mechanical Model for sheet intrusions. Tectonophysics 19.
- Pollard, D.D., and Johnson, A.M., 1973. Mechanics of Growth of some laccolithic intrusions in the Henry Mountains, Utah II: Bending and Failure of overburden layers and sill formation. Tectonophysics, 18.
- Raudsepp, M., . Metagabbro Sill Complex, Favourable Lake Area.
- Robertson, W.D., 1975. Petrology of a Differentiated Ultrabasic Sill from the Cape Smith-Wakeham Bay belt of New Quebec. Unpubl. B.Sc. Thesis, University of Waterloo, p.1-60.
- Roscoe, R., 1952. The viscosity of suspensions of rigid spheres; British Jour. Appl. Physics, v.3, p.267-269.
- Shaw, H.R., 1965. Comments on Viscosity, crystal Settling, and Convection in Granitic Magmas, Am.Jour.Sci., Vol.26, p.120-152.
- Shaw, H.R., 1969. Rheology of Basalt in the Melting Range, Jour. of Petrol. vol.10, no.3, p.510-535.
- Shaw, H.R., 1972. Viscosity of Magmatic Silicate Liquids: An empirical method of Prediction. Am.Jour.Sci. vol.272, p.870-893.

- Shaw, H.R., Wright, T.L., Peck, D.L., and Okamura, R., 1968. The viscosity of basaltic magma: an analysis of field measurements in Makaopuhi Lava Lake, Hawaii. *Am.Jour.Sci.* Vol. 266, p.225-264.
- Simkin, T., 1967. Flow Differentiation in the picritic sills of North Skye, in Wyllie, P.J., ed., *Ultramafic and Related Rocks*; New York, John Wiley and Sons Inc., p.64-69.
- Thompson, D.L., 1976. Viscosity and its Application. Unpubl. Tech. Report. McMaster University, p.1-20.
- Winkler, H.G.F., 1974. *Petrogenesis of Metamorphic Rocks*. Springer-Verlag, p.1-320.
- Wolf, W.J., 1974. Year End Project Report, Kenty Project, Unpubl. Exploration Report, COMINCO LTD.
- Wyllie, P.J. (ed.), 1967. *Ultramafic and Related Rocks*. John Wiley and Sons, Inc., 465 p.

## APPENDIX A

## VOLUME CALCULATIONS

Measurements of the long and short dimensions (a, b) have been made for each grain in thin section (where  $a \geq b$ ). The values of a and b were chosen so as to approximate the area of each grain to a rectangle of equal area, so that a and b do not necessarily always represent exactly the long and short axis. The area of the grain may then be calculated by

$$A = ab$$

to within an accuracy of approximately 10%.

It would be instructive to know the volume of each grain, but unfortunately this is not possible. A semi-quantitative idea of the volume may be found by assuming A to be a minimum area (this can be shown theoretically to be the case) and using the average value of a and b as the third dimension (c) to calculate a minimum volume.

The following method has been used:

1. The most common value of a, b has been found empirically to be 0.7, so that:

$$\text{if } A = ab, \text{ then } b = .7a, a = \sqrt{\frac{A}{.7}} \text{ and } C = \frac{a+b}{2} = .85a$$

Therefore, the values of a, b and c can be found from A.

2. The shapes of the olivine grains in thin section suggests that their 3-D shape can best be thought of as the average of an ellipsoid and a 3-D rectangle. Therefore:

$$V_{\text{average}} = \frac{V_{\text{ellip.}} + V_{\text{rect.}}}{2}$$

Because  $a$ ,  $b$  and  $c$  are related to  $A$ , the final formula should be of the form:

$$V_{\text{average}} = kf(A)$$

where  $k$  is a constant.

This has been found to be:

$$V_{\text{average}} = .774(A)^{3/2}$$

Fig. A graphically depicts the process involved in calculating the area and then the volume from an operator selected measurement of the long and short axis of olivine grains as seen in thin section.

Fig. B is a print of a typical thin section field used in the calculations. In practice measurements were made on an image many times larger.

The average value of  $A$  has been calculated by:

$$\bar{A} = \frac{\sum_{i=1}^n A_i}{n}$$

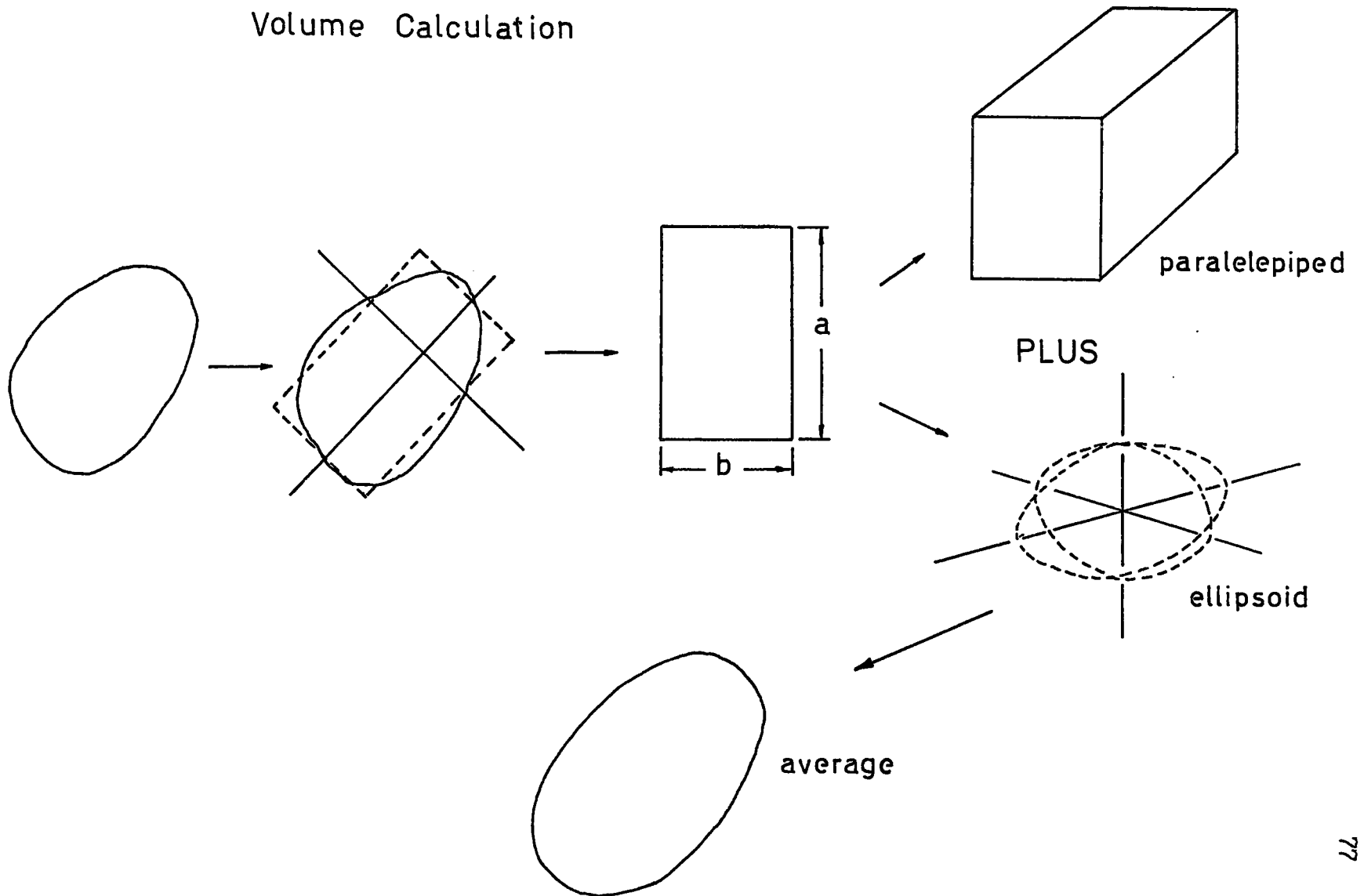
where  $n$  is equal to the number of grain measurements for each individual station.

The  $j^{\text{th}}$   $M$ -factor is calculated by:

$$M_j = \frac{\sum_{i=1}^j A_i}{j}$$

where  $j$  equals the number of grains to be considered i.e. 10, 30 and 50. Therefore  $A_1$  to  $A_j$  are the largest  $j$  grains.

Fig. A Method of Area and Volume Calculation



## APPENDIX B

Contained within Appendix B are the following Tables and Figs.:

A. Grain Size Analyses: Class Interval Frequencies

Table 1. Frequency for Class Interval 0.4 mm<sup>2</sup>

Table 2. Frequency for Class Interval 0.2 mm<sup>2</sup>

Table 3. Frequency for Class Interval 0.1 mm<sup>2</sup>

B. Chemical Analyses

Table 4. Whole Rock Analyses in Weight % Oxides

Table 5. Partial Chemical Analyses in Weight % Oxides

C. Grain Size Histograms

Individual histograms of olivine grain size from each of the thin sections studied. Three class intervals are shown. Figs. 1-14.

D. Sample Number Location

TABLE 1

## GRAIN SIZE ANALYSES

FREQUENCY FOR CLASS INTERVAL  $0.4 \text{ mm}^2$  (normalized to 100%)

Class	B-30	B-31	B-33	B-38	B-40	T-113	T-110	T-109	B-43	T-115	B-44	B-45	T-124
0-0.4	67.48	48.48	53.58	26.28	30.71	36.90	34.43	42.09	33.33	49.62	49.78	43.55	64.42
0.4-0.8	22.77	31.06	25.59	29.93	25.00	25.00	26.41	30.41	30.14	28.18	27.55	30.65	18.87
0.8-1.2	4.07	9.85	8.92	18.97	17.86	15.77	16.62	13.87	15.52	9.98	9.33	13.44	7.16
1.2-1.6	3.25	3.79	4.17	8.02	7.15	9.52	5.19	3.65	4.11	5.49	3.55	6.99	3.25
1.6-2.0	.81	3.03	3.57	6.20	7.86	5.65	5.66	2.92	3.66	3.00	3.11	3.22	1.95
2.0-2.4		3.03	3.57	2.55	4.28	2.38	4.72	2.19	2.74	1.75	.89	.54	1.52
2.4-2.8		.76		2.18	.71	1.49	1.42	2.44	3.20	.25	2.60	.54	.68
2.8-		.76	2.39	5.83	6.42	3.28	7.55	2.45	7.20	1.50	2.65	1.08	1.74

TABLE 2	GRAIN SIZE ANALYSES					FREQUENCY FOR CLASS INTERVAL 0.2mm <sup>2</sup> (normalized to 100%)							
Class	B-30	B-31	B-33	B-38	B-40	T-113	T-110	T-109	B-43	T-115	B-44	B-45	T-124
0-0.2	33.33	18.18	25.60	11.68	10.00	15.77	13.68	18.25	14.61	22.94	26.67	15.59	37.74
0.2-0.4	34.15	30.30	27.98	14.60	20.71	21.13	20.75	23.84	18.72	26.68	23.11	27.96	26.68
0.4-0.6	15.45	21.97	16.07	17.52	18.57	14.29	11.79	18.00	18.72	16.46	16.00	18.28	12.15
0.6-0.8	7.32	9.09	9.52	12.41	6.43	10.71	14.62	12.41	11.42	11.72	11.56	12.37	6.72
0.8-1.0	2.44	7.58	4.76	9.85	7.86	8.63	9.43	8.27	10.50	5.49	4.89	8.60	4.12
1.0-1.2	1.63	2.27	4.16	9.12	10.00	7.14	5.19	5.60	5.02	4.49	4.44	4.48	3.64
1.2-1.4	2.44		2.38	6.20	2.86	3.87	2.83	1.46	2.74	3.74	3.11	6.45	2.82
1.4-1.6	.81	3.79	1.79	1.82	4.29	5.65	2.36	2.19	1.37	1.75	.44	.54	.43
1.6-1.8		.76	2.38	3.65	2.86	3.27	3.77	2.43	3.20	2.00	2.22	1.61	.87
1.8-2.0	.81	2.27	1.19	2.55	5.00	2.38	1.89	.49	.46	1.00	1.33	1.61	1.08
2.0-2.2		.76	1.79	1.09	2.14	1.49	1.42	.97	.91	1.25	.89	.54	.87
2.2-2.4	.81	2.27	.60	1.46	2.14	.89	3.30	1.22	1.83	.50			.65
2.4-2.6				1.82		.89	1.42	.49	1.83	.25	1.30	.54	.22
2.6-2.8		.76		.36	.71	.60		1.95	1.37		1.30		.43
2.8-3.0		.76	1.19	.36	1.43		.47	.49	.91	.25	.44		.22
3.0-3.5	.81		.60	1.46	.71	.60	.94		2.28	.50	.89	.54	.65
3.5-4.0			.60	.73	2.14	.30	2.36		1.37		.44	.54	.22
4.0-5.0				1.82	.71	1.49	1.42		1.37	.25	.44		.65
5.0-				1.46	1.43	.85	2.36		1.37	.50	.44		

TABLE 3

## GRAIN SIZE ANALYSES

FREQUENCY FOR CLASS INTERVAL 0.1 mm<sup>2</sup> (normalized to 100%)

Class	B-30	B-31	B-33	B-38	B-40	T-113	T-110	T-109	B-43	T-115	B-44	B-45	T-124
0-0.1	15.45	3.03	6.55	2.92		2.98	4.25	4.14	3.65	5.74	12.89	3.78	18.22
0.1-0.2	17.89	14.39	19.05	8.76	10.00	12.80	9.43	14.11	10.96	17.21	13.78	11.83	19.52
0.2-0.3	17.89	15.91	14.88	6.93	10.00	13.69	11.32	12.41	11.87	15.49	9.78	13.98	15.62
0.3-0.4	16.26	14.39	13.10	7.60	10.71	7.74	9.43	11.44	6.85	11.22	12.89	13.98	11.06
0.4-0.5	9.76	11.36	9.52	8.03	7.14	6.25	5.66	11.19	7.31	9.48	12.44	12.37	6.07
0.5-0.6	5.69	10.61	6.55	9.49	11.43	8.04	6.13	6.81	11.42	6.98	3.56	5.91	6.07
0.6-0.7	4.07	5.30	4.17	6.57	2.86	8.33	9.43	5.84	5.48	6.48	4.44	7.53	3.47
0.7-0.8	3.25	3.79	5.36	5.84	3.56	2.36	5.19	6.57	5.94	5.24	7.11	4.84	3.25
0.8-0.9	1.63	5.30	2.38	4.74	4.29	4.17	5.66	4.62	6.39	3.74	4.00	4.84	1.95
0.9-1.0	.81	2.27	2.38	5.11	3.56	4.46	3.77	3.65	4.11	1.75	.89	3.76	2.17
1.0-1.1	.81	1.52	2.38	5.11	7.14	4.17	1.89	2.92	3.20	2.00	3.11	2.15	1.74
1.1-1.2	.81	.76	1.79	4.01	2.86	2.98	3.30	2.68	1.83	2.45	1.33	2.69	1.30
1.2-1.3	.81		1.19	4.01	.71	1.19	.47	1.22	.91	1.75	1.78	3.23	.87
1.3-1.4	1.63		1.19	2.19	2.14	2.68	2.36	.24	1.83	2.00	1.33	3.23	1.95
1.4-1.5	.81	3.03	.60	.36	2.86	3.57	.94	1.46	.46	.50	.44	.54	.22
1.5-1.6	.81	.76	1.19	1.46	1.43	2.08	1.42	.73	.91	1.25			.22

TABLE 4

## WHOLE ROCK ANALYSIS IN WEIGHT % OXIDES

	B-29	B-31	B-33	B-38	B-43	B-45
SiO <sub>2</sub>	42.56	41.12	39.04	38.42	39.46	42.28
Al <sub>2</sub> O <sub>3</sub>	13.51	9.84	5.52	12.20	2.57	6.91
FeO	11.14	8.71	6.43	4.00	6.29	10.29
Fe <sub>2</sub> O <sub>3</sub>	0.79	4.76	6.03	7.62	7.94	2.38
TiO <sub>2</sub>	0.31	0.31	0.36	0.21	0.21	0.26
CaO	6.92	4.74	3.60	1.72	2.86	2.76
MgO	17.37	23.03	30.05	26.55	31.13	26.18
Na <sub>2</sub> O	0.13	0.11	0.04	0.04	0.04	0.04
K <sub>2</sub> O	0.06	0.08	0.04	0.04	0.04	0.06
L.O.I.	7.31	7.82	9.39	9.57	9.64	9.13
TOTAL	100.24	100.59	100.59	100.47	100.27	100.50

TABLE 5

## PARTIAL CHEMICAL ANALYSES IN WEIGHT % OXIDES \*

## BRAVO ULTRAMAFICS

	B-30	B-32	B-34	B-35	B-36	B-37	B-39	B-40	B-41	B-42	B-44	B-46
MgO	22.58	27.31	31.31	34.96	34.96	33.50	33.50	33.86	34.96	33.50	28.40	20.75
Fe <sub>t</sub>	9.50	9.61	9.58	8.83	7.60	8.83	9.61	9.05	7.04	8.16	10.11	7.66
SiO <sub>2</sub>	41.90	39.52	38.50	38.72	38.84	38.08	38.10	38.62	39.38	39.10	39.30	48.04
S	.180	.06	.120	.07	.021	.041	.026	.034	.130	.120	.052	.002
Ni <sub>t</sub>	.066	.115	.09	.115	.115	.135	.125	.140	.150	.150	.100	.082
Ni <sub>s</sub>	.033	.065	.087	.09	.09	.105	.10	.095	.150	.150	.050	.002
Cu <sub>t</sub>	.006	.008	.008	.001	.004	.005	.003	.005	.004	.002	.003	.001

\* Fe<sub>t</sub> - Iron total

Ni<sub>s</sub> - Nickel in sulfides

### C. Grain Size Histograms

#### i) Histogram Key

#### ii) Individual Histograms

B - 30

B - 31

B - 33

B - 38

B - 40

T - 75 - 113

T - 75 - 110

T - 75 109

B - 43

T - 75 - 115

B - 44

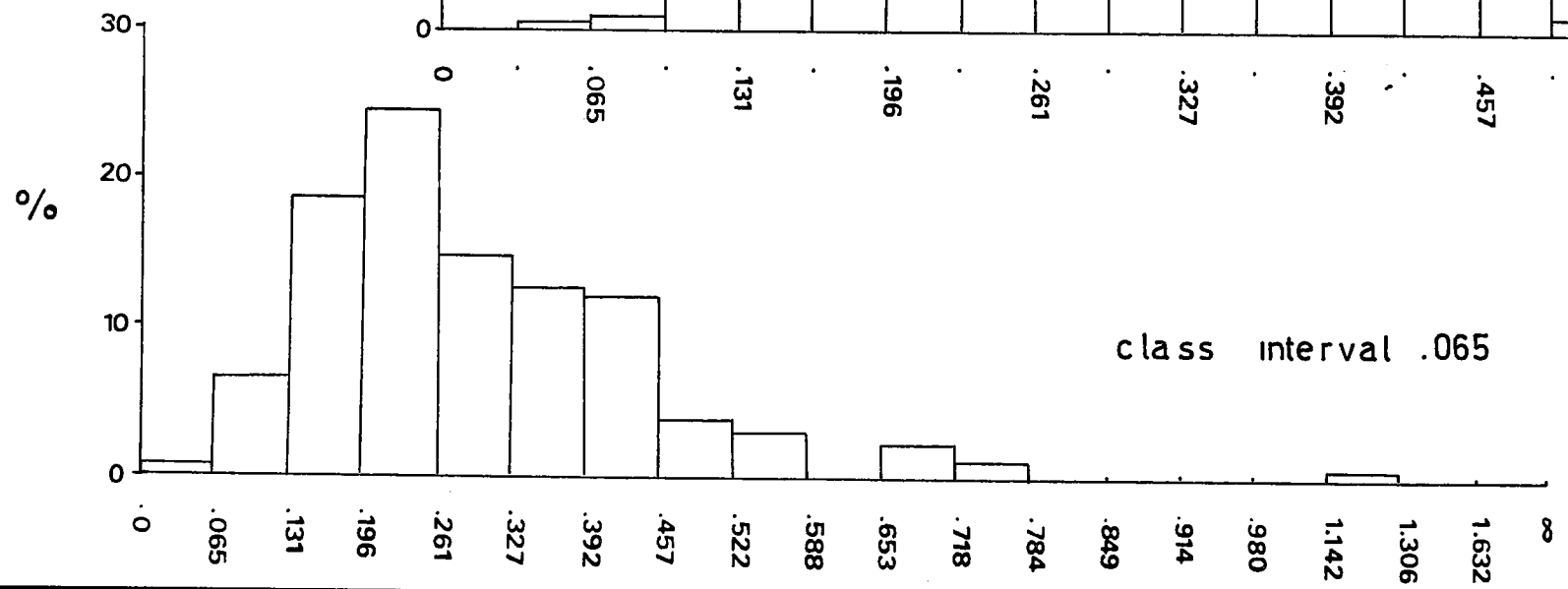
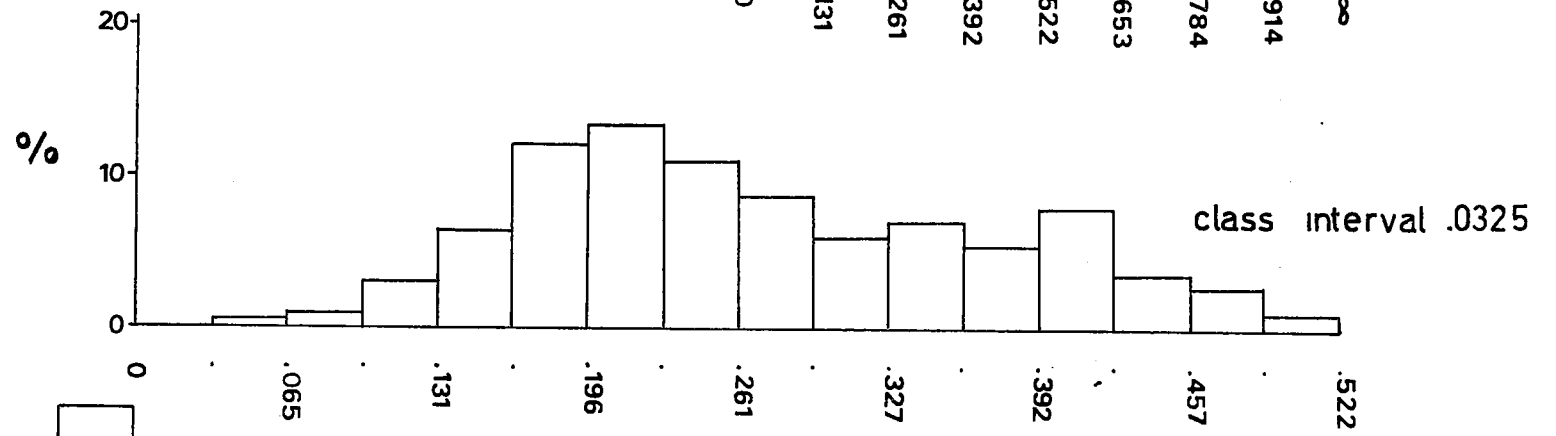
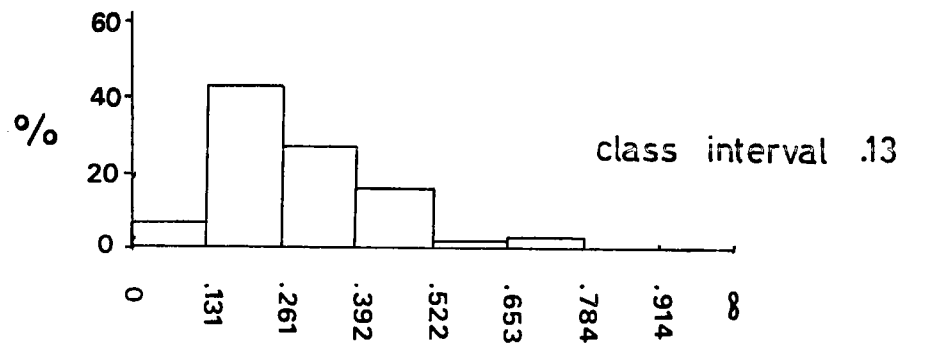
B - 45

T - 75 - 124

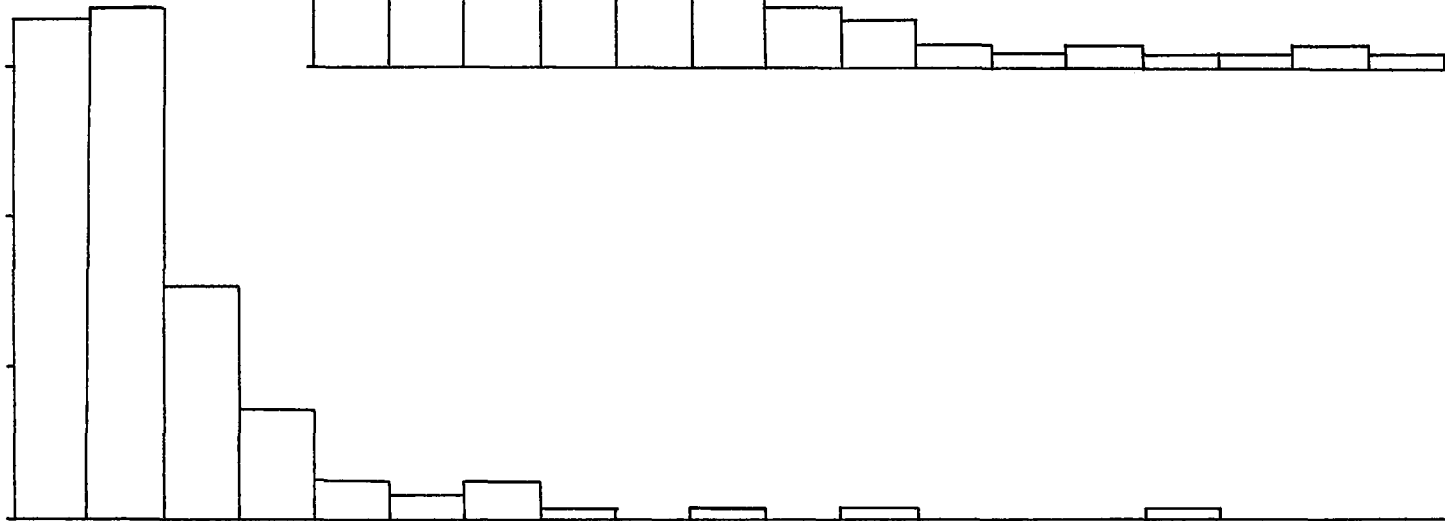
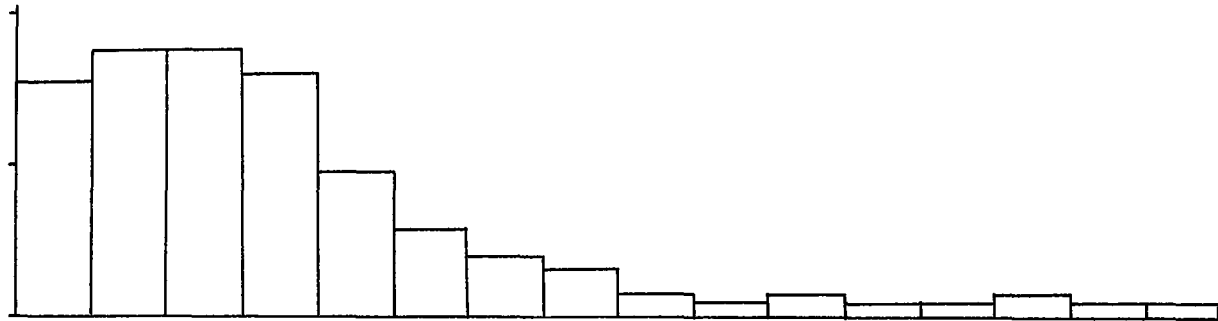
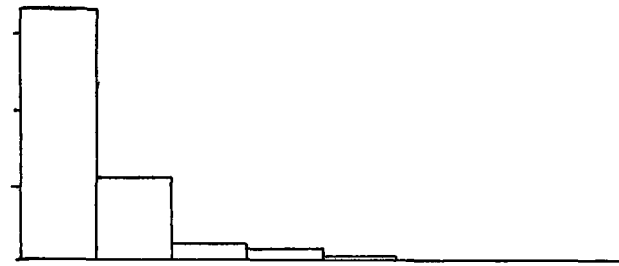
T : my sample

B : Cominco sample

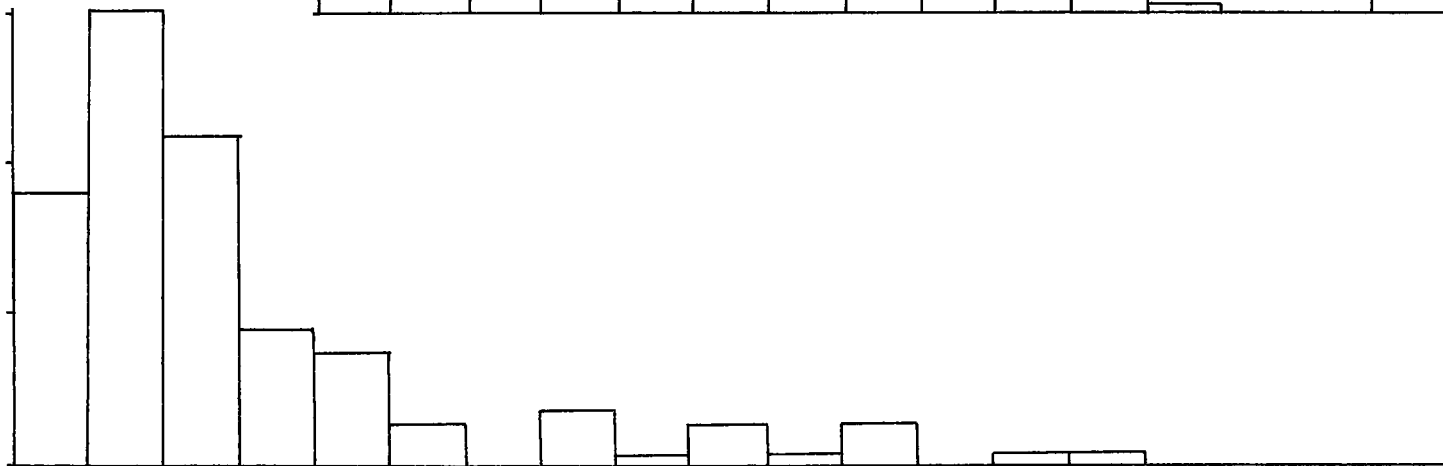
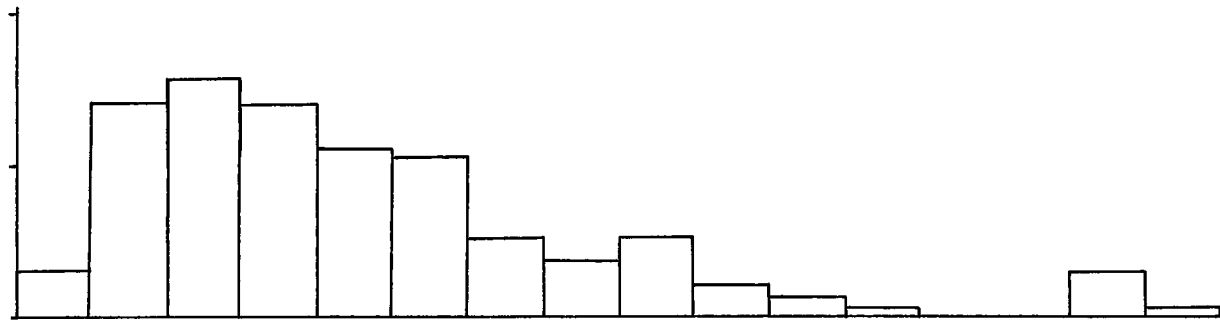
HISTOGRAM KEY  
 %Frequency vs Area  
 area in mm<sup>2</sup>



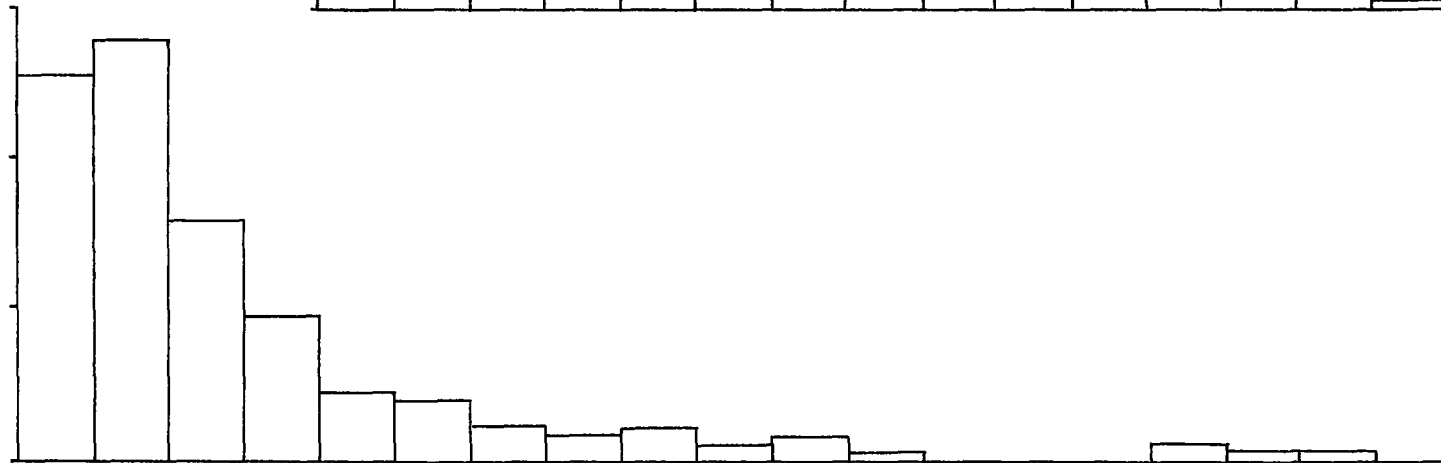
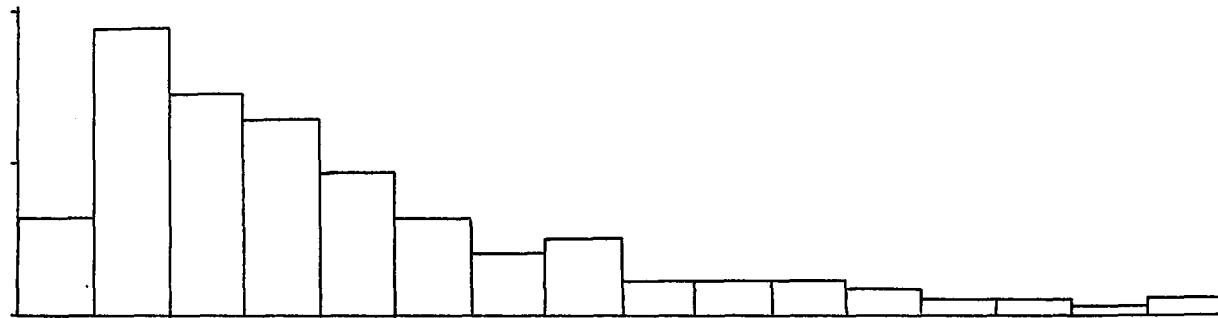
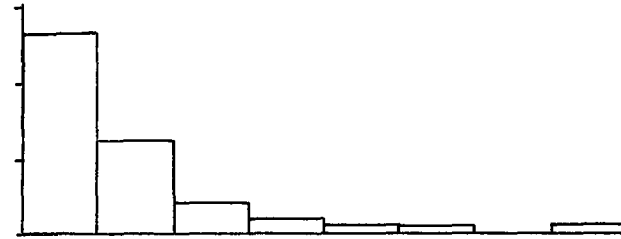
Sample B-30



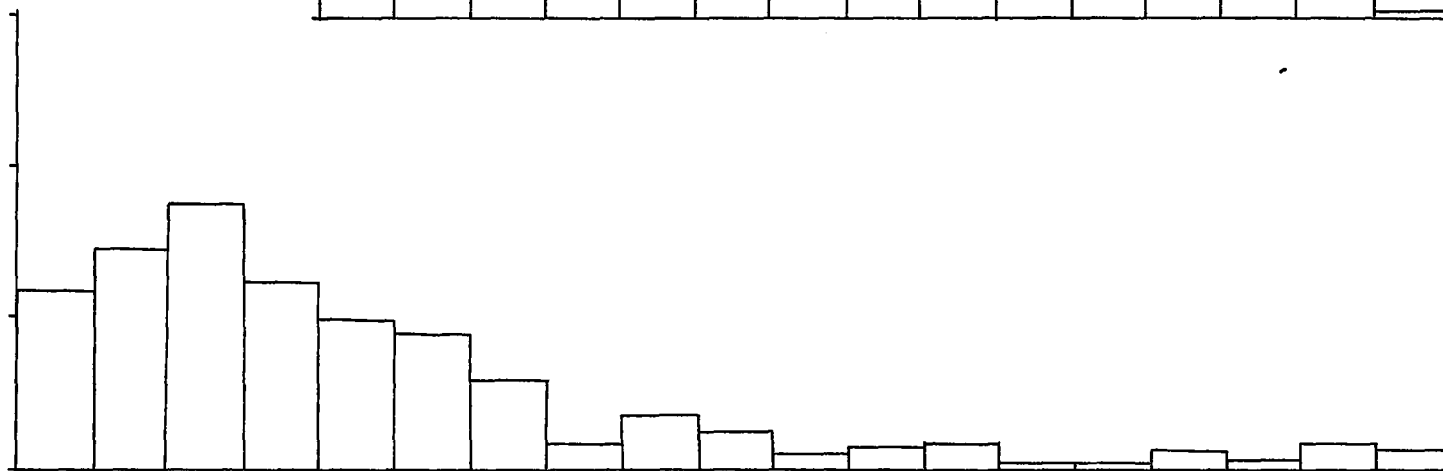
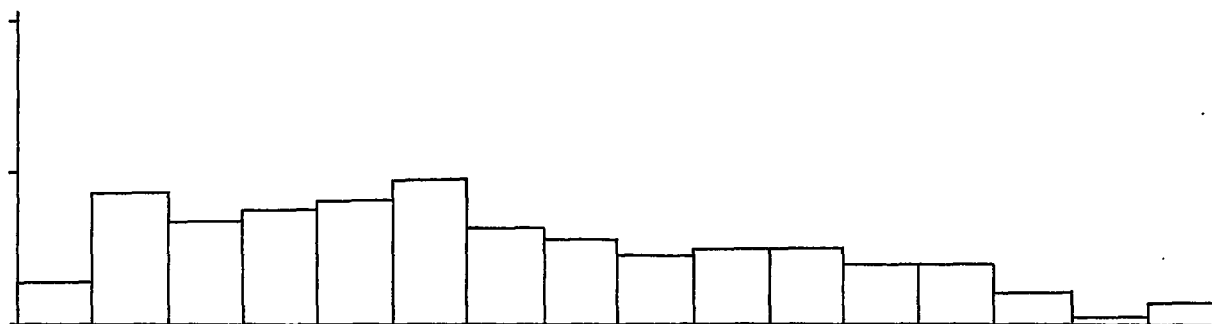
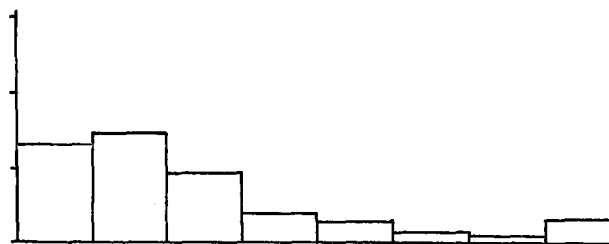
Sample B-31



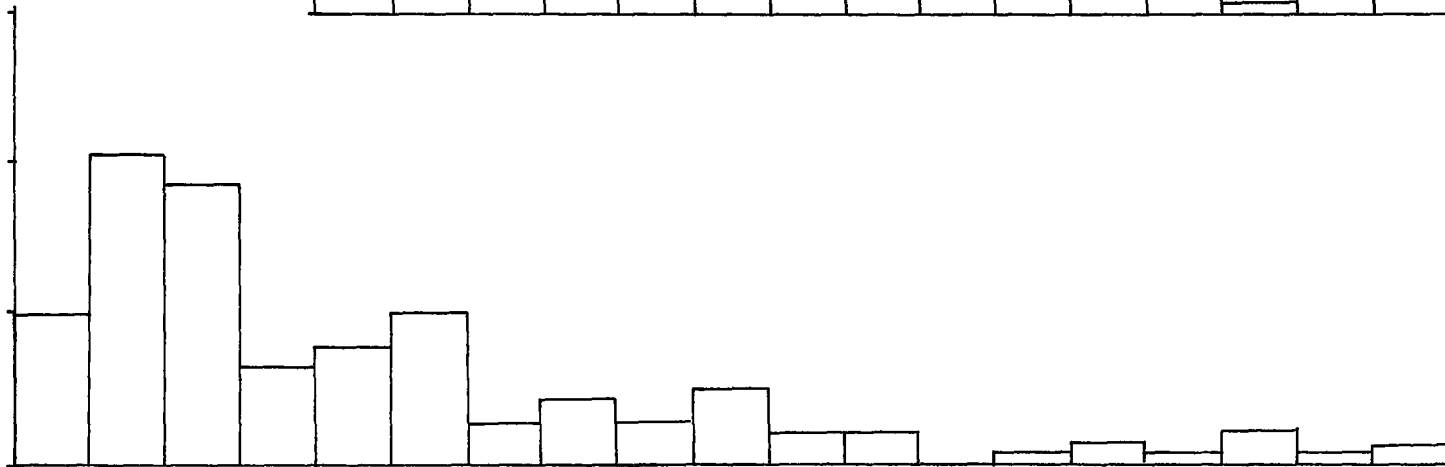
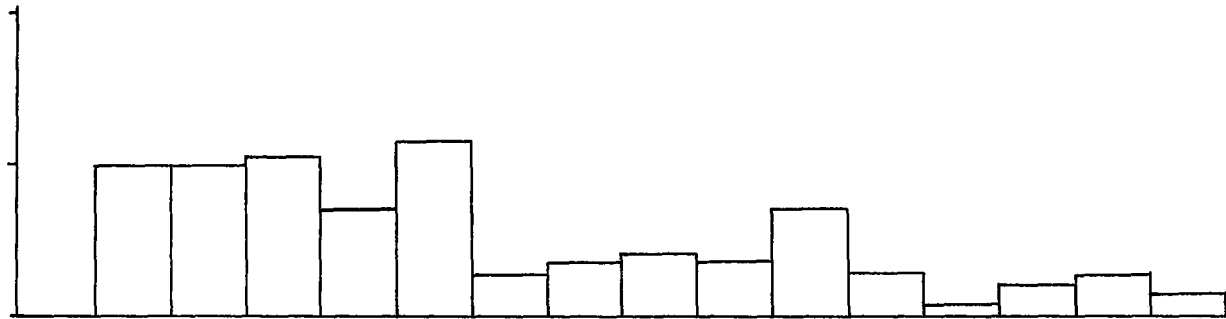
Sample B-33



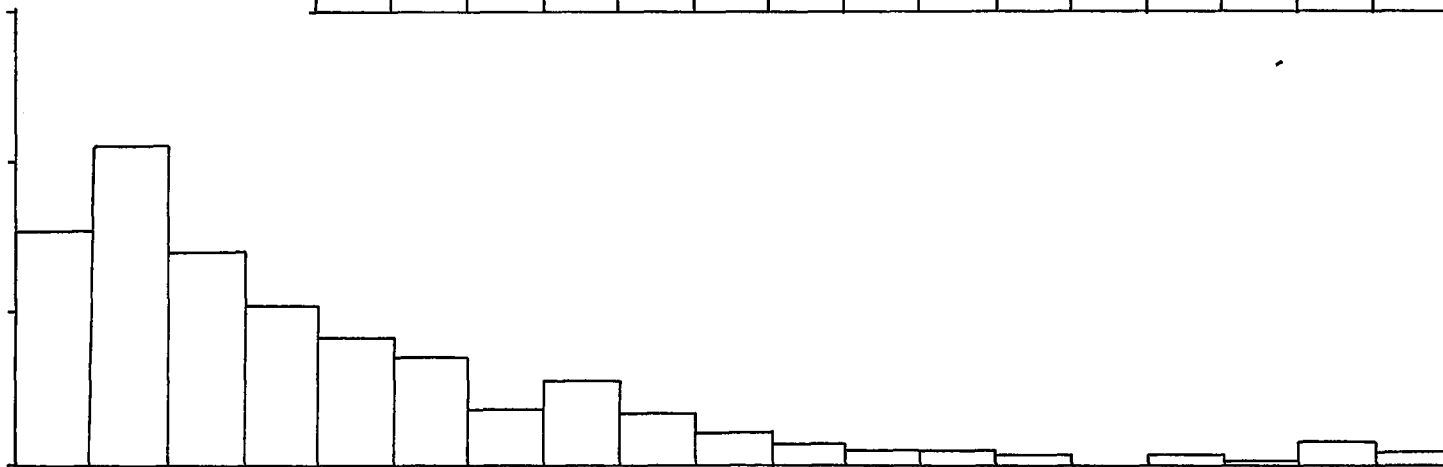
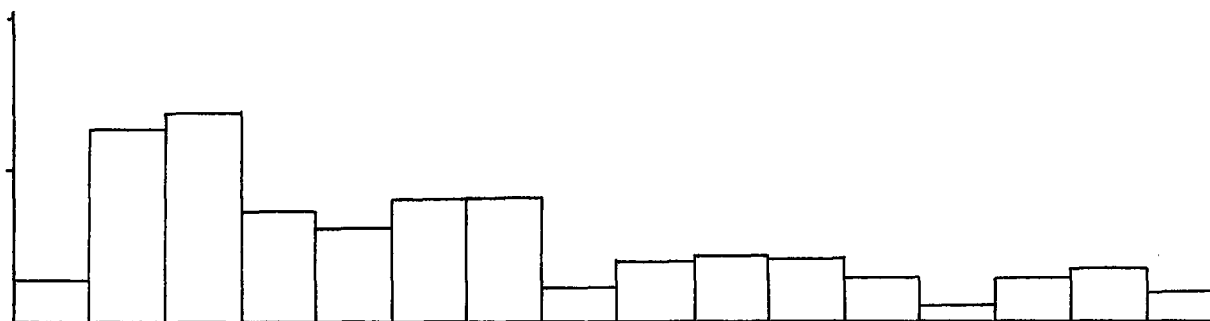
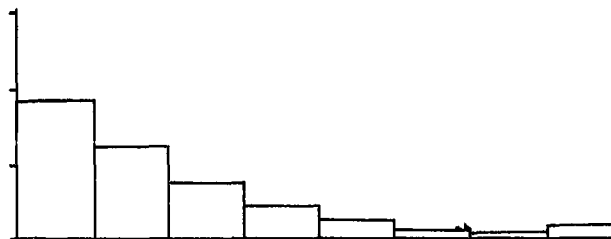
Sample B-38



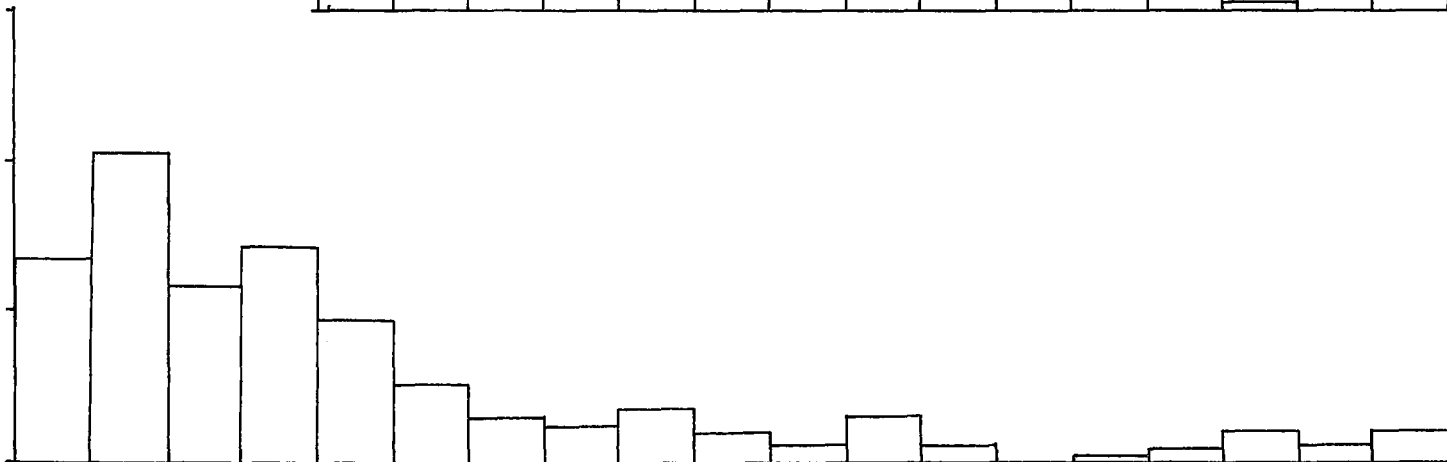
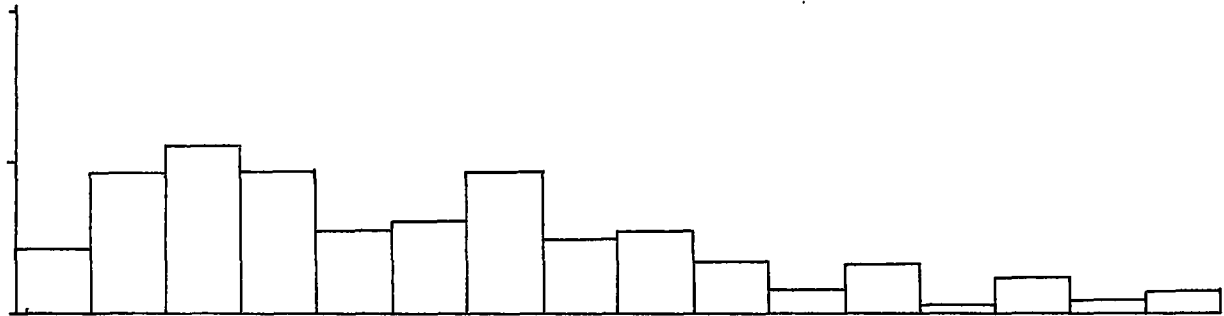
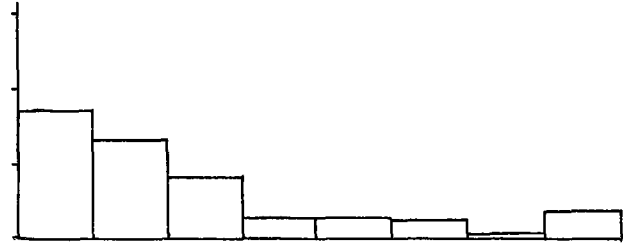
Sample B-40



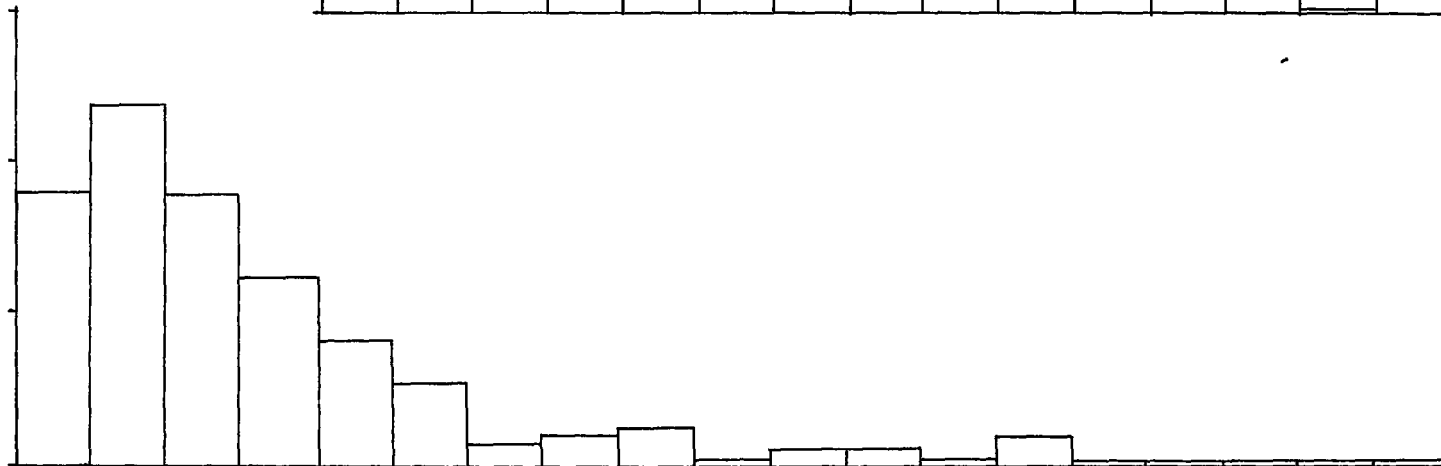
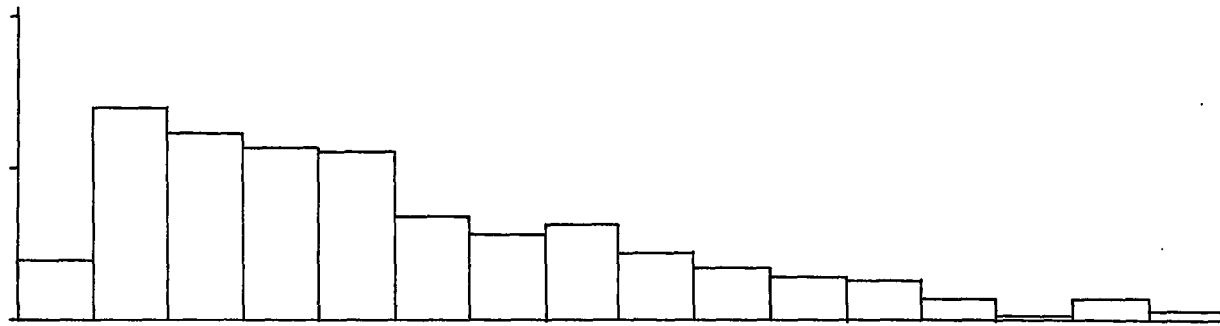
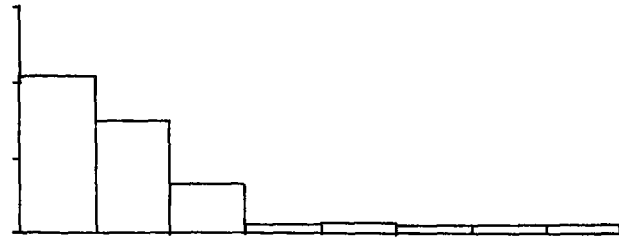
Sample T-75-113



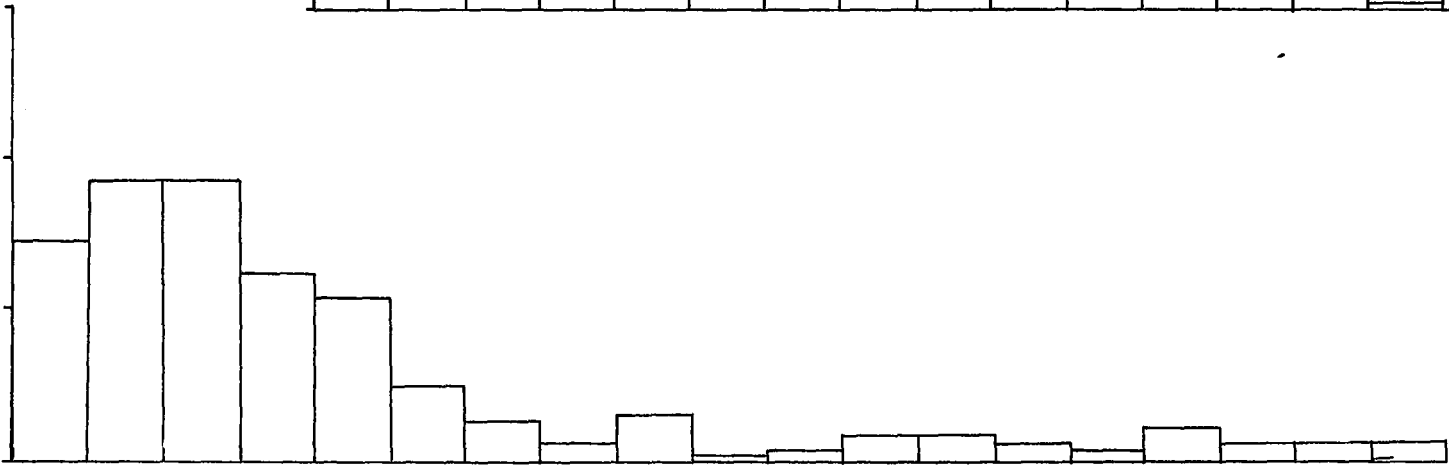
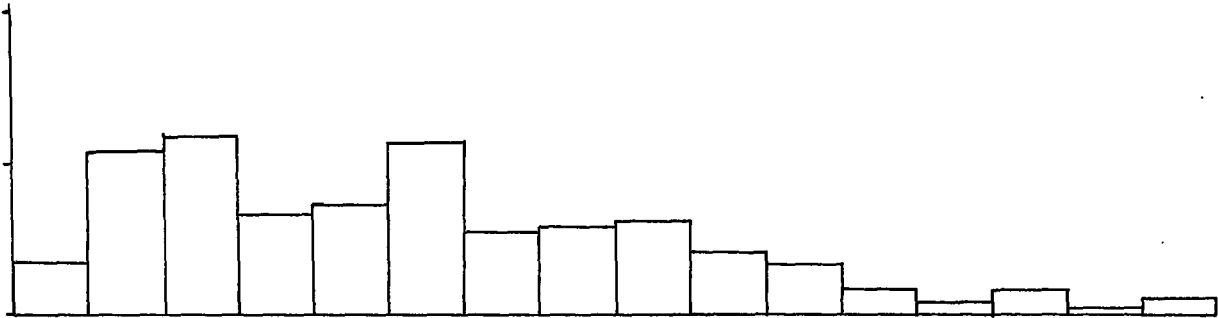
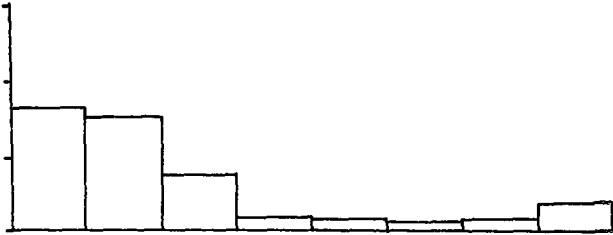
Sample T-75-110



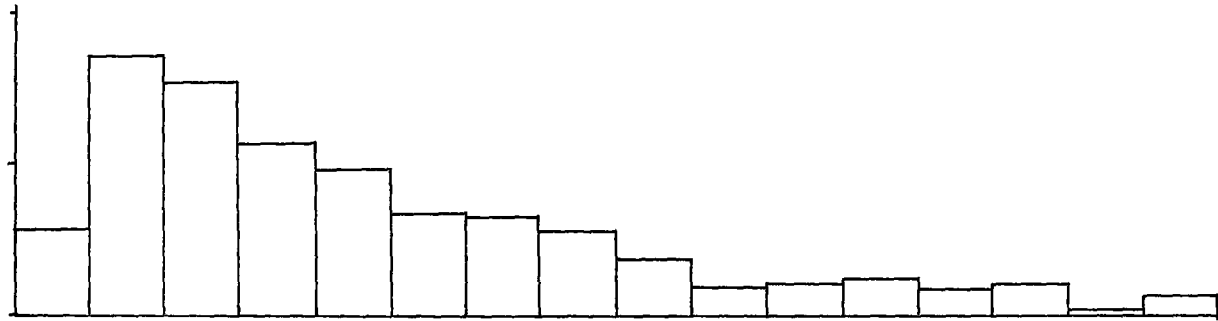
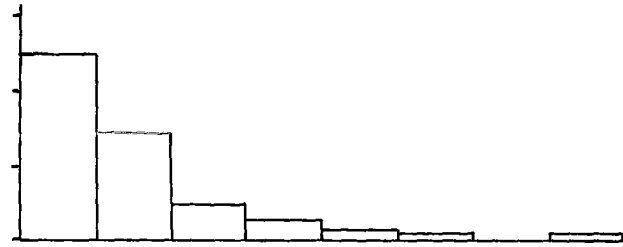
Sample T-75-109



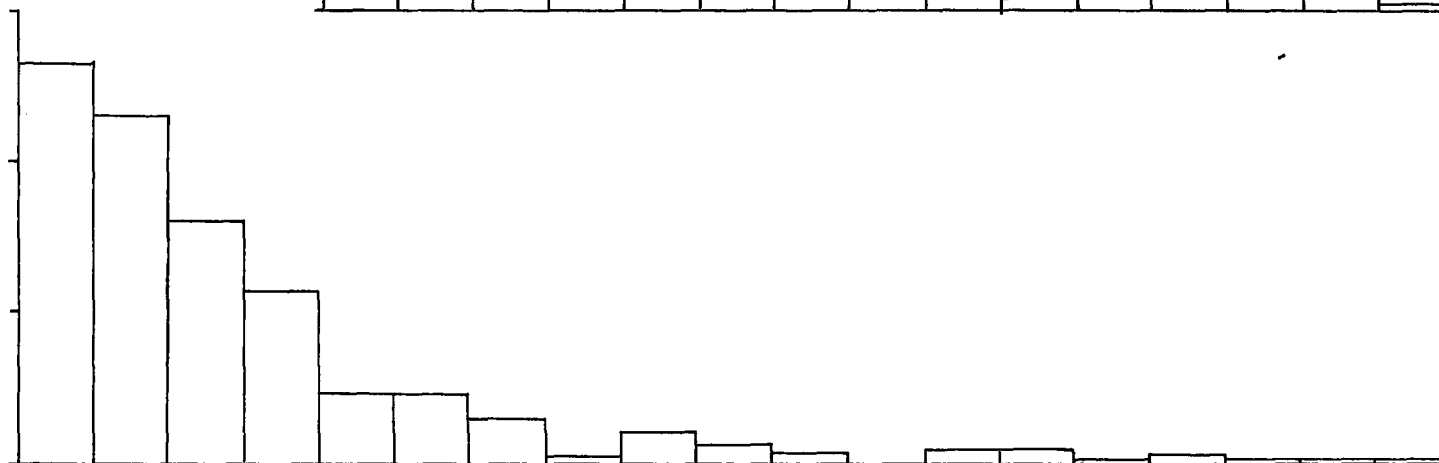
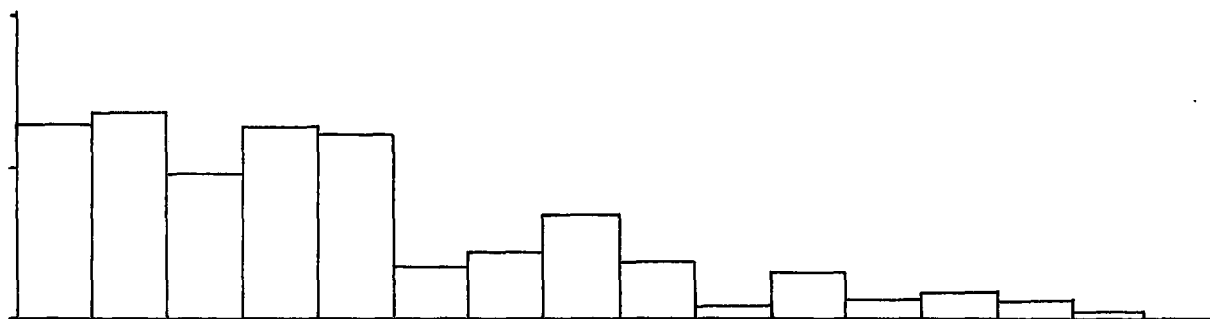
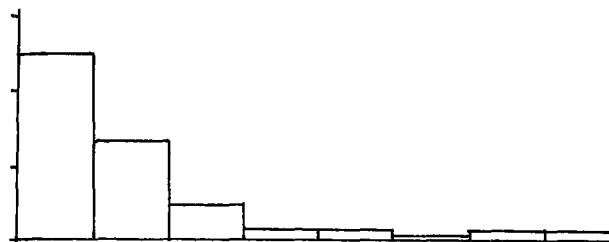
Sample B - 43



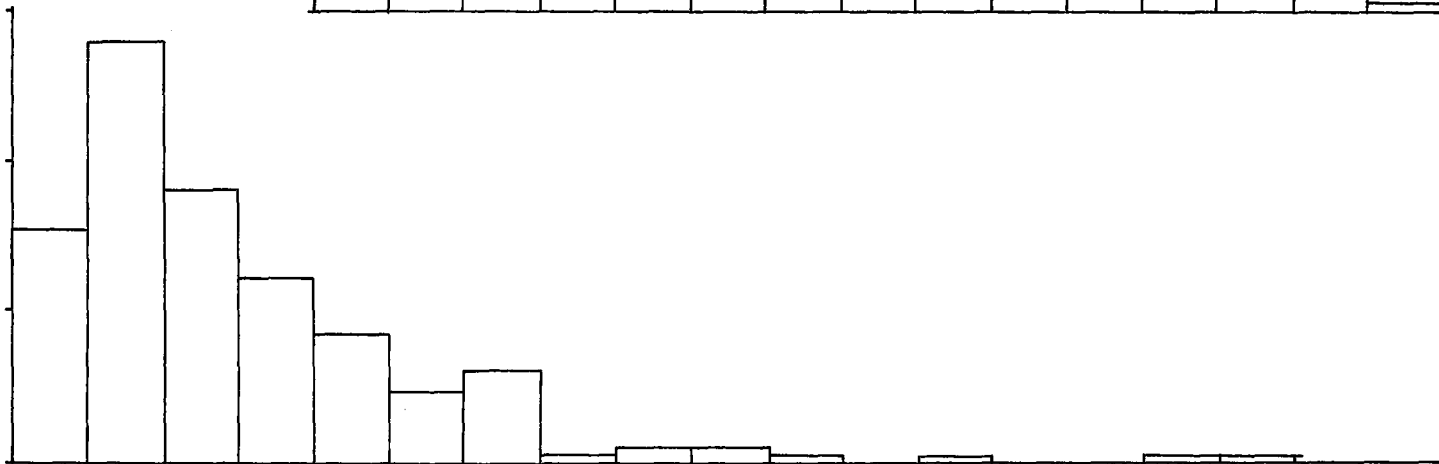
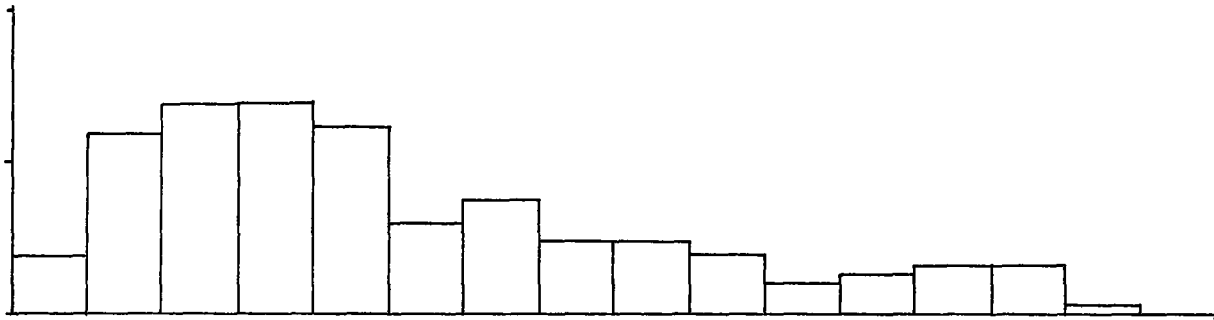
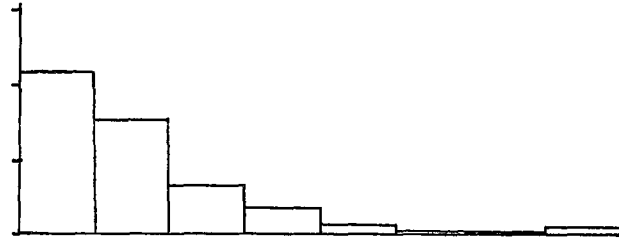
Sample T-75-115



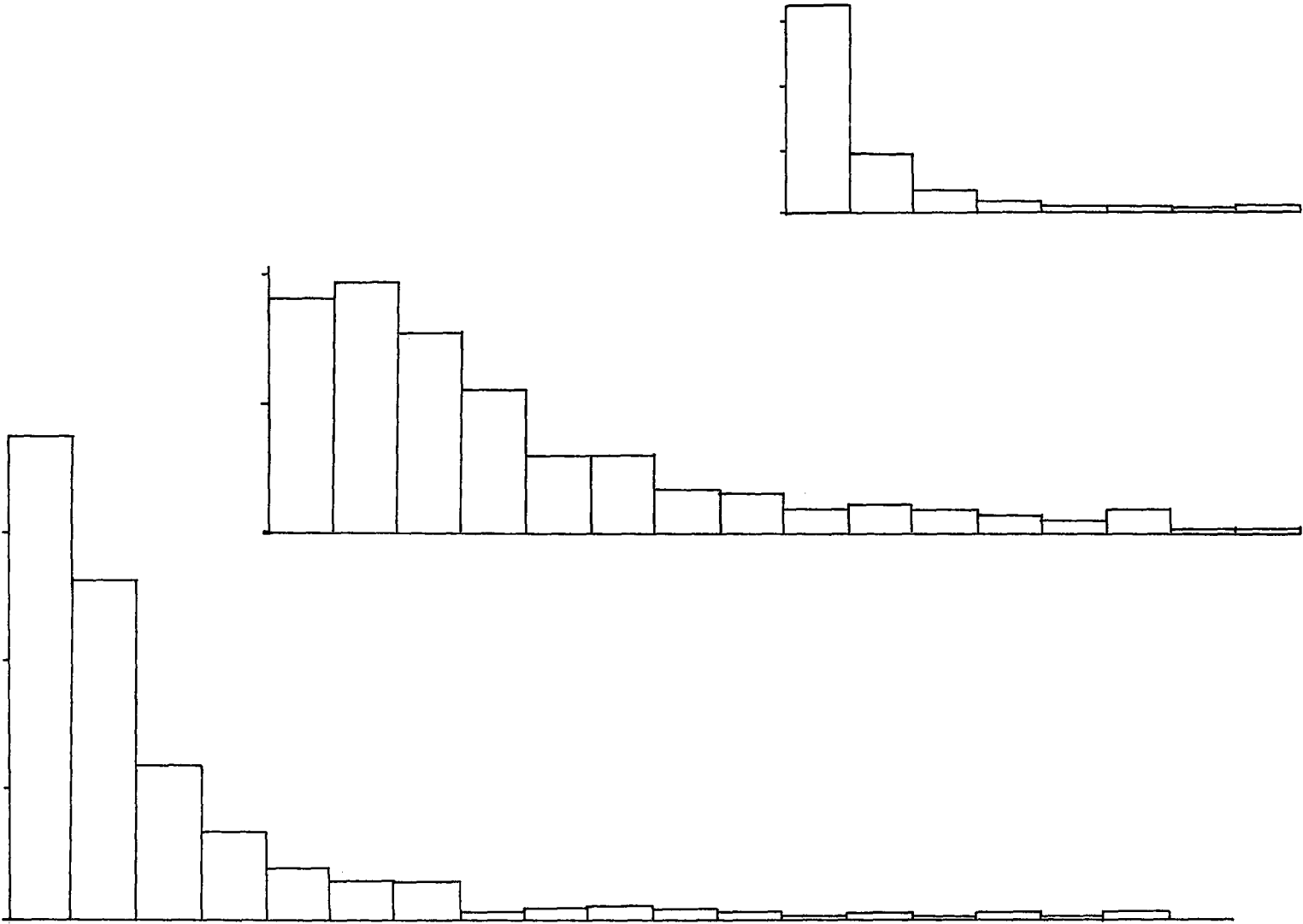
Sample B-44



Sample B-45



Sample T-75-124



Appendix B part D  
Sample Number Location

